The contribution of geochemistry to ancient harbor geoarcheology: The example of Ostia Antica

Hugo Delile, Jean-Philippe Goiran, Janne Blichert-Toft

The contribution of geochemistry to ancient harbor geoarcheology: The example of Ostia Antica

H. Delile[1*], J.-P. Goiran[1], J. Blichert-Toft[2]

[1]Maison de l'Orient et de la Méditerranée, CNRS UMR 5133, 69365 Lyon Cedex 7, France

[2] Ecole Normale Supérieure de Lyon, Université Claude Bernard-Lyon I, CNRS UMR 5276, 69007 Lyon, France

*****Corresponding author

Contact details:

7 rue Raulin - 69365 LYON cedex 7, France

+33 (0)6 82 73 66 53

hugo.delile@mom.fr

Abstract

Once trapped in ancient harbor basins, sediments form environmental archives that have been widely studied by geoarcheologists in recent decades, especially to help reconstruct fluvio-marine landscapes of the last millennia. In some cases, classic environmental markers cannot be used for this purpose either because of their scarcity in the sedimentary deposits, or because analytical costs limit the resolution that can be achieved. In order to remedy these shortcomings, and to complement the more commonly used proxies, elemental and isotopic geochemistry has been added to the geoarcheological toolkit. Here we show how to "read" the evolution of the paleo-environmental dynamics in the water column of Ostia Antica (Rome's first maritime harbor) using the geochemical and isotopic record of a 3000-year-old sediment core drilled in the ancient harbor basin. A comparison of the results obtained from Ostia Antica with those of other ancient Mediterranean harbors reveals the nature of the main environmental processes operating during the formation of sedimentary deposits in harbor

basins. From this comparative approach, it appears that the respective weight of each control factor is dependent on the coastal geomorphological context of the sites where the harbors were established. Since the discovery of the harbor of Ostia Antica in 2014, this method has provided the means, for the first time, to identify two distinct harbor basin regimes; an initial marine-dominated regime from the middle of the 4th c. BC to ~ the 3rd c. BC, and a later freshwater-dominated regime up to the 2nd c. BC. More generally, we observe the effects of the dynamics of the deltaic progradation of the Tiber, which very early on was subject to a hydro-climatic component, on the processes of alluviation of the harbor basin. Additionally, and also for the first time in harbor geoarcheology, Pb isotope compositions measured specifically on uncontaminated sediments demonstrate their utility for both identifying the geological sources of the sediments of the Tiber delta and discriminating finer from larger particles. The present study further provides an opportunity to test the validity of two hypotheses recently put forward: (1) that a series of three tsunamis is recorded in the harbor silts, and (2) that an initial lagoon-type harbor was constructed at Ostia Antica, which later evolved into a fluvial harbor. Neither of these hypotheses are supported by the present data.

Keywords: Rome, Ostia Antica, ancient harbor basins, geoarcheology, sedimentology, geochemistry, Pb isotopes, Tiber river

1. Introduction

When harbor geoarcheology emerged as a discipline at the beginning of the 1990s following the excavations of the ancient harbors of *Caesarea* (Israel) (Reinhardt et al., 1994, 1998; Reinhardt and Raban, 1999) and Marseille (France) (Hesnard, 1994; Morhange, 1994; Morhange et al., 2001, 2003), the analytical and investigative methods used were based on those well known from other domains within the earth sciences, such as micropaleontology

(molluscs, ostracods, foraminifera, diatoms, pollen) and sedimentology (texture, granulometry, exoscopy) (Goiran and Morhange, 2003; Marriner and Morhange, 2007; Bravard, 2009; Cubizolle, 2009). Two decades later, while these well-tested methods continue to be used in the field, elemental and isotopic geochemistry has been added successfully to the geoarcheology toolkit, as we show below.

Although geochemistry began to be used in harbor geoarcheology in the mid-2000s to determine human impact based on findings of ancient metal traces (Le Roux et al., 2003, 2005; Véron et al., 2006, 2013, 2018; Marriner and Morhange, 2007; Stanley et al., 2007; Delile et al., 2014b, 2015, 2016b, 2017), it had not so far been used in paleo-environmental studies. It is only very recently that research teams, primarily from Germany, have used elemental geochemistry to improve on paleo-environmental reconstructions in archeological contexts. Important examples of such work carried out on ancient harbors are the studies of Oiniadai (Vött, 2007), Olympia (Vött et al., 2011), Palairos-Pogonia (Vött et al., 2011), Corinth (Hadler et al., 2013a), Kyllini (Hadler al., 2015b), and Alkinoos (Finkler et al., 2018) in Greece; Ephesus (Stock et al., 2013, 2014, 2016; Delile, 2014; Delile et al., 2015) and Elaia (Shumilovskikh et al., 2016) in Turkey; *Portus* and Naples in Italy (Delile et al., 2014a, 2016a); and Magdala (Rossi et al., 2015) in Israel. This recent expansion of geochemistry into geoarcheological research is a direct result of the widespread use of micro-XRF core scanners during the last decade. This technology can rapidly, non-destructively, and automatically scan sediment cores to produce elemental profiles at high resolution, which contribute greatly to the reconstruction of paleo-environments (Croudace and Rothwell, 2015). However, to take full advantage of this technique, it is indispensable to have prior knowledge of the geochemical properties of the sediments in question in order to avoid misinterpretations. One such common mistake consists in using certain elemental ratios capable of tracing the sedimentological (e.g. Zr/Rb and Zr/Ti applied as particle size proxies) or environmental (e.g.

Sr/Al, Mg/Ca or Ca/Al, and Si applied as biological production proxies or Mn/Fe, U, and Mo applied as water ventilation proxies) parameters without taking into account the geological, hydrological, and climate contexts of the sites under study, each of which can significantly modify the meaning of these ratios. Initially, the use of geochemistry for reconstructing environmental processes was applied to (i) marine sediments to decipher paleo-productivity, deep water ventilation, and paleo-temperatures, and (ii) lacustrine sediments to track atmospheric pollution, human impact, paleo-climatic changes, aeolian input, paleo-floods, catchment weathering, and source rock compositions (Boyle, 2002; Croudace and Rothwell, 2015).

Here, we discuss the types of environmental and anthropogenic processes that are most likely to benefit from the use of high-resolution geochemistry applied to the geoarcheological study of ancient harbors. To that end, we identify the geochemical fingerprints of the main environmental and anthropogenic processes that took place in the ancient harbor basin of Ostia Antica and compare them with:

(i) the "classic" environmental archives documented so far by geochemistry (i.e., lacustrine and marine sediments);

(ii) the "traditional" proxies used in harbor geoarcheology (see above), especially those applied to Ostia Antica's ancient harbor basin, which are well documented from a paleo-environmental perspective (Goiran et al., 2012, 2014, 2017; Hadler et al., 2015a; Sadori et al., 2016; Wunderlich et al., 2018);

(iii) those identified at *Portus* (Delile et al., 2014a for the Trajanic basin and this study for the Claudius basin), Ephesus (Delile et al., 2015), and Naples (Delile et al., 2016a).

Although micropaleontological (ostracods, foraminifera, pollen) and sedimentological (texture, granulometry) studies have been carried out on the harbor deposits of Ostia Antica, the dynamics and paleo-environmental changes in its water column remain poorly understood.

Improving this understanding is all the more important since Ostia Antica had a river harbor located a short distance from the mouth of the Tiber River, which was to subject it to both marine and river influences (Goiran et al., 2012, 2014, 2017; Salomon et al., 2016). As a result, in the present work, we focus in particular on the interaction between fluvial and marine impacts on the harbor water column.

2. Study area

2.1. Archeological and historical background

According to Roman historians, Ostia Antica was founded during the reign of Ancus Marcius in the 7th c. BC. However, the *castrum* (building, or plot of land, used as a fortified military camp) did not appear before the 4th or beginning of the 3rd c. BC (Coarelli, 1988; Martin, 1996; Zevi, 2002; Brandt, 2002). The absence of evidence for the earliest periods has led to hypotheses about the existence of a paleo-Ostia, the location of which remains unknown and would correspond to the city founded by Ancus Marcius (Coarelli 1988; Martin 1996; Zevi 2002; Brandt 2002). Ancient texts reveal that the harbor of Ostia Antica became a commercial and military port during the Punic wars (Livy, 45, 22) and played a vital role in providing Rome with food supplies (especially olive oil from Spain and grain from the North African provinces) during the 1st c. BC (Le Gall, 1953; Zevi, 2001b). Nevertheless, at this time, Puteoli (Pozzuoli) on the Bay of Naples remained the principal maritime port of Rome for trade (Balland, 1965). It was considered to be one of the busiest centers of trade in the Roman Empire, especially for metal ingots, for which a route from the Cartagena/Mazarron and Rio Tinto mines in Spain to Puteoli and Rome was heavily used (Domergue and Rico, 2014; Delile et al., 2016b). The large distance separating the ports of Puteoli and Ostia Antica, as well as a problematic massive siltation of Ostia's harbor basin caused by a succession of floods discharging sediments at the mouth of the Tiber (Strabo, 5, 3, 5), combined with the need to accommodate an increasing number of merchant and military ships arriving from the

Roman provinces, were the main factors that led to the foundation of the new *Portus* harbor complex 3 km north of Ostia Antica in the middle of the 1st c. AD (Keay et al., 2005; Goiran et al., 2014) (Fig.1A).

2.2. Geography and geology

The Tiber delta constitutes the outlet for the water and sediment discharges of a river 405 km long which drains a watershed surface area of 17,375 km², comprising young sediments from the Apennines and modern volcanic deposits in Latium. The annual deposition of sediment in the Tyrrhenian Sea, estimated at 7.2 million tons per year (Iadanza and Napolitani, 2006), has resulted in the construction of a wave-dominated delta 150 km² in extent. The Tiber delta can be divided into (i) the eastern inner deltaic plain, related to the paleo-lagoons of Maccarese in the north and Ostia in the south; (ii) the western outer deltaic plain, where the landscape is composed of accreting dunes to which must be added the submerged area; (iii) the deltaic front (mainly composed of sand and silt); and (iv) the prodelta (mainly composed of mud and clay) (Salomon, 2013; Salomon et al., 2017).

The geomorphological evolution of the Tiber delta during the Holocene period is well documented (Bellotti et al. 1994, 1995, 2007, 2011; Giraudi, 2004; Milli et al., 2013; Salomon, 2013; Salomon et al., 2018). During the periods of the Republic and the Empire, the position of the Tiber mouth likely was located close to the Boacciana Tower (Tomassetti 1897) (Fig.1B). Additional information about the coastline comes from the immediate surroundings of *Portus* (Arnoldus Huyzendveld, 2005; Giraudi, 2004; 2009; Salomon, 2013) and from south of the Tiber delta, on the Laurentine shore (Bicket et al., 2009). However, during the Imperial period, the rapid seaward progression of the coastline recorded by the Tiber delta, which could have been more active at the river mouth, is the cause of relatively poor paleo-geographical knowledge of the Tiber mouth and its dynamics during Roman times. This rapid evolution explains why discovering the exact location of the ancient port of Ostia

Antica has been so controversial until recently (Goiran et al., 2012). The harbor of Ostia Antica, which has been dated to the period of the Republic, was initially difficult to identify, and its infrastructure (i.e., docks for loading and unloading of goods) could have been located anywhere along the riverbanks in direct connection with the city and its storage facilities (warehouses). But since 2012, a large body of multidisciplinary research combining the work of archeologists, historians, geographers, sedimentologists, geomorphologists, micro-paleontologists, and palynologists has confirmed the location of the river mouth harbor basin of Ostia Antica in the northern part of the city, to the west of the "Palazzo Imperiale", founded between the 4th and 2nd c. BC (Goiran et al., 2012, 2014, 2017). The stratigraphy of the cores (Goiran et al., 2014) clearly shows the deposit of harbor silts (dated at their base to the middle of the 4th century BC) at a depth of between 5.7 and 9 m below ground level (m *b.g.l.*) (unit B1, Fig. 2) (i.e., between 3.3 and 6.6 m below present sea level (m *b.p.s.l.*) or between 2.5 and 5.8 m below ancient sea level (m *b.a.s.l.*). The sea level between AD 230-450 was defined locally at 0.8 m ± 10 cm below the current biological sea-level by Goiran et al. (2009)). These harbor silts indicate a calm environment with low-energy currents in which the fluvial influence is reflected in the ostracod assemblages (Fig. 2).

As shown by Salomon et al. (2016), the stratigraphy of the PO2 core can be considered representative of Ostia's harbor area as a whole because of (i) its central location in the harbor basin area; (ii) the limited size of this port basin (~ 0.5 ha) in comparison with that of other ancient harbors (for example the Trajanic basin is ~ 39 ha and that of Ephesus in Turkey ~ 20 ha); (iii) the consistency of its stratigraphic successions deduced from their spatial correlation with other cores drilled in the harbor (Goiran et al., 2014; Hadler et al., 2015); (iv) the spatial extension of these stratigraphic successions to the entire harbor basin area as inferred from geophysical investigations (Hadler et al., 2015a; Wunderlich et al., 2018); (v) its large number

of radiocarbon dates; and (vi) the extraction of the PO2 core by using a rotary mechanical corer that provides cores of a quality superior to those extracted by percussion corers.

3. Materials and methods

We analyzed at high resolution one (PO2, Fig. 1B) of the two cores drilled by Goiran et al. (2014) which led to the discovery of the first harbor of Rome at Ostia Antica. This 12 meter long core was drilled in a low-lying area without any archeological structural remains near the present-day Tiber River (Fig. 1B).

3.1. Radiocarbon dates and the age-depth model

The chronostratigraphic framework of the PO2 core is based on 15 radiocarbon dates (Goiran et al., 2014, 2017; Sadori et al., 2016; Delile et al., 2017) for which the age-depth model was created using the Clam software (Blaauw, 2010) (Fig. 2). The details of the age-depth model and the ^{14}C dates, as well as the inherent uncertainties associated with both, can be found in Delile et al. (2017), who exercised great caution in the use of these ages by applying them only to broad historical periods (Republic, High and Late Roman Empire, etc.).

The singular S-shape of the ^{14}C age-depth model of the PO2 core (Fig. 2) is typical of ancient harbor deposits and due to the dredging practices used at the time. This well-known phenomenon in Mediterranean harbors, well documented at Ostia by Goiran et al. (2014, 2017) and Salomon et al. (2016), is discussed in section 4.4.1.

3.2. Analysis of major and trace elements

The geochemical analyses were carried out on the entire core with high sample resolution (86 samples analyzed, i.e., one sample approximately every 14 cm). The data are published in Delile et al. (2017) together with the analytical techniques, which are also briefly summarized here. First, the sediments were sieved at 63 µm with a nylon sieve instead of a metal sieve in order to avoid potential contamination. After drying, 100 mg of sieved

198 sediment from each core sample was dissolved at the Ecole Normale Supérieure de Lyon in a
199 clean laboratory under laminar flow hoods. The samples were digested in a 3:1:0.5 mixture of
200 concentrated double-distilled HF, HNO_3, and $HClO_4$ in Savillex beakers left closed on a
201 hotplate at 120-130 °C for 48 h, then evaporated to dryness. Perchlorates and any remaining
202 fluorides were converted to chlorides by drying down several times with 6 M distilled HCl.
203 The samples in solution in 6 M distilled HCl were all clear, indicating complete sample
204 breakdown. The samples were re-dissolved in 2 ml concentrated distilled HNO_3, from which
205 ~10 percent aliquots were further diluted to 2% HNO_3 and internal standards (10 ppm Sc for
206 ICP-AES and 2 ppb In for Q-ICP-MS) added. Major elements were analyzed by ICP-AES
207 (ICAP 6000) and trace elements by Q-ICP-MS (Agilent 7500 CX). The upper limit of the
208 blank contribution was negligible for major elements and <2% of the sample content for trace
209 elements. The precision on major and trace elements is between 2 and 5%.

210 *3.3. Analysis of Pb isotopes*

211 The method used is described in detail in Delile (2014) and Delile et al. (2014b, 2015, 2016b,
212 2017) and the main steps summarized in the following. After sieving at 63 µm as described
213 above, representative aliquots of 500 mg of sediment were leached with Suprapur chloroform
214 to separate the labile (or anthropogenic) component of the Pb. A second mild leaching step
215 was performed with dilute double-distilled HBr to further recover the most easily displaceable
216 (presumably anthropogenic) Pb, not all of which could be assumed to have been retrieved by
217 chloroform. The leftover sample residues, constituting the natural “geological” Pb, were
218 discarded. The two leachate fractions were combined and their Pb separated on anion-
219 exchange columns using HBr to elute the sample matrix and distilled 6 M HCl to elute the Pb.
220 The sample residues were not measured in this study because the isotopic composition of the
221 natural Pb background had already been determined in a previous study (Delile, 2014; Delile
222 et al., 2014b). The Pb isotope compositions were measured by MC-ICP-MS (Nu Plasma 500

HR) at the Ecole Normale Supérieure de Lyon using Tl doping and sample-standard bracketing (Albarède et al., 2004) and the values for NIST 981 of Eisele et al. (2003). The total procedural Pb blank was < 20 pg, far inferior to the multiple μg of Pb leached and separated from each sample. The external reproducibility of the reported Pb isotope ratios as estimated from the repeated (every two samples) runs of NIST 981 are 100-200 ppm (or 0.01-0.02%) for ratios based on 204 ($^{206}Pb/^{204}Pb$, $^{207}Pb/^{204}Pb$, $^{208}Pb/^{204}Pb$) and 50 ppm (or 0.005%) for $^{207}Pb/^{206}Pb$, $^{208}Pb/^{206}Pb$, and $^{207}Pb/^{208}Pb$. The Pb isotope data published in Delile et al. (2017) were used exclusively to focus on Pb anthropogenic excesses, while here we use the same data set to understand the natural, as opposed to the anthropogenic, Pb isotopic signal.

4. Results and discussion

4.1. Defining the main geochemical fluxes of harbor basin deposits

As mentioned in the introduction, the main objective of this work is to apply multi-elemental analysis to the silico-clastic deposits of the ancient harbor basin of Ostia Antica in order to identify the main inputs and processes involved in their formation. Because the composition and relative weight of different geochemical fluxes reflects the environmental conditions at the time of deposition, we can associate them with environmental variables whose evolution over time enables reconstruction of the paleo-environmental changes that occurred at the scale of the harbor site. For these purposes, the identification of the geochemical fluxes and their associated elementary compositions is a critical aspect requiring great caution.

4.1.1. The three main geochemical inputs and their arbitrarily associated elements

According to Sageman and Lyons (2003), three main inputs are involved in the formation of sedimentary deposits: (i) detrital, (ii) authigenic, and (iii) biogenic materials (Fig. 3).

(i) *Detrital material* (Fig. 3A) is derived from erosion of continental crust and volcanic rocks. These erosion products are carried by the hydrological network from their sources at the watershed to the marine environment. The principal elemental components of the particle flux transported by modern fluviatile sources are, in order of decreasing abundance, Si, Al, Fe, Ca, K, Mg, Na, Ti, P, Mn, and Ba, according to Martin and Whitfield, 1983. However, inter-comparison of these elements within the PO2 core shows stratigraphic distributions (see panel showing detrital elements in Fig. 3A) that differ from those predicted. This qualitative observation is reproduced quantitatively using the correlogram (Fig. S1) which displays relatively weak levels of correlation between, for example, Al and K ($r = 0.31$), Mg and Fe ($r = 0.06$), and Ti and Ba ($r = 0.2$), even though positive correlations between some elements qualified as detrital, such as Al, Mg, Zr, and Ti, are also observed. These first-order observations demonstrate that it is incautious to use *sensu stricto* certain elements considered to be universal markers of detrital origin. These differences between observation and theory in the chemical composition of the detrital fraction are accounted for by the relative weight of the local specificities that directly affect the factors controlling the composition in question: the mineralogy of the enclosing rocks, the erosional regime which itself depends on regional climate conditions (temperature, precipitation, and runoff), and the reactivity of eroded material during transport (Sageman and Lyon, 2003).

(ii) *Authigenic material* (Fig. 3B) is controlled by the redox state of the system, which depends on the ventilation conditions of bottom waters which in turn determines organic and inorganic reactions by which dissolved constituents are precipitated as minerals, either as metal oxyhydroxides (O_2 enrichment) or metal sulfides (O_2 depletion). The control factors of authigenic material in sediments depend mainly on the water-column mixing rate and the production of organic matter. The redox state usually is tracked by certain elements such as Fe, S, V, Mo, and U (Sageman and Lyon, 2003), which are assumed to be enriched under

reducing conditions and depleted under oxidizing conditions. All of them correlate negatively with Mn because Mn is enriched under oxidizing conditions and depleted under reducing conditions. However, as seen in Fig. 3, the behavior of these elements as a function of stratigraphy does not show such a distribution. This qualitative observation is consistent with the quantitative observation as the correlogram in Fig. S1 shows relatively weak correlations between, for example, Mo and U (r = 0.07), V and Mo (r = 0.2), and U and S (r = 0.2), even if positive correlations are also observed, especially between Mo and Fe (r=0.55), Fe and U (r=0.51), Fe and V (r=0.75), and Fe and S (r=0.8) (Fig. S1). None of these elements, therefore, can be used as universal markers of authigenic inputs.

(iii) *Biogenic material* (Fig. 3C) reflects the photosynthetic production of organic material and the presence of remains of skeletal material, the latter being composed of calcite ($CaCO_3$) or silica (SiO_2). Biogenic fluxes in the sedimentary system depend on the concentration and supply of nutriments from surface waters (nitrate, phosphate, and micro-nutriments such as Fe). They are produced by chemical erosion and terrestrial biogenic activity or biological processes in the water column. Usually, the biogenic flux is tracked by Si, Ca, Sr, P, or Loss on Ignition (L.O.I.) (Sagement and Lyons, 2003; Sánchez Vizcaíno and Cañabate, 1999; Delile et al., 2016a). However, as observed for the detrital and authigenic fluxes, neither the qualitative nor the quantitative observations (Figs. 3C and S1) show clear systematic positive or negative correlations between, for example, Ca and Sr (r = 0.04), Ca and P (r = -0.3), and Sr and P (r = 0.3).

This attempt at classification, or grouping, of chemical elements taken individually according to the three principal inputs involved in the formation of sedimentary deposits (Fig. 3) has revealed the limits of the approach. First, assigning a given element to a specific category of inputs is not supported by robust statistic correlations, hence calling for caution in automatically using geochemical proxies traditionally considered to be robust tracers for

297 particular inputs. Second, the individual observation of several dozen chemical elements is
298 fastidious work without any real added value. For these reasons, the reading of the underlying
299 causes of geochemical variation and their number is difficult.

300 *4.1.2. A new way to define the main geochemical fluxes of harbor basin deposits*

301 In order to examine in-depth the thousands of data acquired by multi-element analysis (39
302 chemical elements measured) at high resolution (86 samples analyzed in the present study),
303 we use factor analysis in order to convert data into uncorrelated and limited variables, also
304 known as factors. The factors resulting from the statistical treatment of the full data set (39
305 elements for 86 samples) carry a large part (>75%) of the total geochemical variability of the
306 depositional system. These factors in turn correspond to variables that are equivalent to the
307 principal components deduced from the PCA statistical procedure (see Appendix A in Delile
308 et al., 2014a). Based on the loading values of each factor (Fig. 4A), the distribution of the
309 chemical elements, which results from positive (element clusters located in the same position
310 relative to the y-axis) and/or negative (element clusters located in the opposite position
311 relative to the y-axis) correlations, enables us to determine the environmental variable
312 expressed behind each factor.

313 Based on this method, we discriminate four main factors controlling the bulk of the
314 geochemical composition of the PO2 core (Fig. 4):

315 (i) *The first factor* (47% of the total variability of the geochemical signal, Fig. 4)
316 comprises elements associated exclusively with a siliciclastic detrital flux (Th, Zr, U, K,
317 REEs, etc.) and is marked with negative F1 values. All these elements are known to be
318 enriched in the Roman Alkaline Province in Italy, including the downstream volcanic rocks of
319 the Tiber River watershed, where they show the highest abundances in floodplain sediments
320 (De Vos and Tarvainen, 2006). This volcanic province is also known under the name of the

Roman Magmatic Province – Latian District (RMP-LD) (Mattei et al., 2010) which regroups the Colli Albani, Vulsini, Cimini, Vicano, Ceriti, and Sabatini volcanoes, all very close to the Tiber delta. The RMP-LD region, which is one of four major volcanic provinces of the Tyrrhenian margins of peninsular Italy, consists of mafic ultrapotassic rocks with a remarkably homogeneous elemental composition characterized by high abundances of Pb, Th, U, Ce, and La and low abundances of Ti, P, Ta, and Nb (Mattei et al., 2010). These geochemical features distinguish all the volcanoes close to the Tiber delta. This is shown in Fig. 4A where elements with affinities for the RMP-LD mafic ultrapotassic rocks show strongly negative values (ranging between -0.7 and -1), whereas elements depleted in the same rocks display significantly lower negative values (ranging between -0.5 and 0).

The main characteristic of Factor 1 is that it tracks the sedimentary units with the coarser particles, since the lowest F1 values occur in the sandy units A and B2 (Figs 2, 4B). The correlogram for elementary and granulometry data (Fig. S2) from harbor units only (units B1 and B2) shows that the sandy fraction is clustered within these elements (Th, Zr, U, K, REEs, etc.). We conclude from this that Factor 1 reflects siliciclastic terrigenous influence which, in terms of depositional environment, corresponds to the ancient hydrodynamic conditions of the harbor water column.

(ii) *The second factor* (13% of the total variability of the geochemical signal, Fig. 4) opposes elements indicative of detrital fluxes (other than the siliciclastic detrital flux of F1) (Ga, Al, Rb, Li, Ti, Mg, etc.) to elements indicative of a carbonate component (Ca). The detrital component (positive F2 values) clearly reflects another type of terrigenous influence, that related to aluminosilicates. Al, Ga, Rb, Li, Mg, and Ti are strongly correlated among themselves (Fig. S1) because they are all constituents of clay minerals (De Vos and Tarvainen, 2006). Figure S2 confirms the predominance (weight) of fine particles in Factor 2 because the hierarchical clustering shows good correlations between clays and silts containing

346 these elements. Factor 2 reflects the terrigenous influence of aluminosilicates which,
347 interpreted in terms of an environmental variable, corresponds to the ancient quiet
348 hydrodynamic conditions of the harbor water column.

349 (iii) *The third factor* (10% of the total variability of the geochemical signal, Fig. 4)
350 presents with negative F3 values elements associated with authigenic fluxes (redox
351 conditions), especially those tracking oxygen depletion in the water column (S, Fe, Mo, V).
352 Factor 3 also includes chalcophile elements that precipitate as sulfides under anoxic
353 conditions (Pb, Cu, Co, Sb). This factor also has been recorded in the ancient harbor deposits
354 of Ephesus (Delile et al., 2015).

355 (iv) *The fourth factor* (7% of the total variability of the geochemical signal, Fig. 4)
356 opposes Na to heavy metals such as Sn, Cd, and Pb. The strong influence of Na within the
357 stratigraphy reflects either the salinity of the harbor itself or the invasion of the sediments by
358 the salt wedge. For the Trajanic harbor as well as for that of Ostia Antica, the association of
359 the ostracodal marine group with high sediment Na content unambiguously reveals a marine-
360 dominated environment (Delile et al., 2014b; Goiran et al., 2014; Sadori et al., 2016) for the
361 basal part of core PO2 (Figs. 2, 4B). This marine influence is opposed mainly to the inputs of
362 heavy metals derived from human activities (Sn, Cd and Pb). Since marine influence is not
363 associated with any trace metal pollutants, we conclude that anthropogenic pollutants were
364 carried by the freshwater of the Tiber River (Delile et al., 2017). This is supported by the
365 ostracodal freshwater group, which increases greatly in the upper part of unit B1 (Fig. 2).
366 Owing to Factor 4, we can show for the first time that the functional harbor unit B1 recorded
367 two distinct regimes (gray dotted line in Fig. 4B): a harbor basin under marine influence at a
368 depth of about 9 to 7 m *b.g.l.* (i.e., 4.6-6.6 m *b.p.s.l.* or 3.8-5.8 m *b.a.s.l.*) followed by an
369 increasingly fluvial-dominated regime at a depth of about 7 to 6 m *b.g.l.* (i.e., 3.6-4.6. m
370 *b.p.s.l.* or m 2.8-3.8 m *b.a.s.l.*).

4.2. Synthesis of the main environmental factors leading to the formation of ancient harbor basin deposits in the Mediterranean

The methodological tool associating elemental geochemistry with factor analysis in order to improve the reconstruction of paleo-environments has been applied to four other roman harbor basins in the Mediterranean besides that of Ostia Antica used as an example above: that of Ephesus in Turkey (Delile et al., 2015), that of Naples in Italy (Delile et al., 2016a) and those of Trajan (Delile et al., 2014a) and Claudius (this study) at *Portus*. Table 1 presents the first synthesis of this method in describing the different environmental variables (that is, the factors identified by factor analysis) that affected the paleo-environmental dynamics of the water columns of these ancient harbor basins, as well as their respective weights expressed in percentages. F1 corresponds to the most important control factor, often representing around 50% of the variance, while F4 constitutes the least significant environmental variable with values of less than 10% (Table 1).

According to Table 1, the first environmental component (42%) that affects the paleo-environmental dynamics of harbor water columns corresponds to detrital fluxes, that is, sedimentary discharge from an outlet. This is not surprising as all these harbor sites, except that of Naples, are located on deltas that are sub-aqueous and sub-aerial coastal accumulations of river-derived sediments. The process of construction of these complex coastal landforms is based on the terrigenous detritus of fluvial origin, the effectiveness of which increases at river mouths, where the ancient harbor basins are located. This principal environmental characteristic of harbor environments is also present in the typology of ancient harbors produced by Giaime et al. (2016). According to the statistical applications (Principal Component Analysis and Hierarchical Ascendant Classification) on which their typology rests, the major natural process that distinguishes between specific types of harbors is the rate of sediment supply. This process moreover is responsible for the major constraint on

navigation as it reduces the draught for ships in the harbor basins because of siltation and alluviation (Goiran and Morhange, 2003; Marriner and Morhange, 2007; Salomon et al., 2016; Goiran et al., 2017). The predominance of detrital fluxes in the paleo-environmental evolution of the water column in harbor basins is subject to the coastal geomorphology of the sites where these harbors were established, as only those located at deltas are dominated by this environmental parameter. Indeed, the paleo-environmental changes of the water column of the ancient harbor of Naples, located in a small coastal bay, were affected more by aeration (Factor 1 = redox conditions = 36%) than by terrigenous contributions (Factor 2 = 16%) (see Table 1 and/or Delile et al., 2016a). In general, these detrital fluxes are composed of siliciclastic and aluminosilicate minerals which cause enrichment in Al, Zr, Ti, Th, Mg, Ba, K, Co, Zn, and REEs in the sediments. This category of flux generally reflects the ambient hydrodynamics of harbor basins in which the recrudescence of currents is produced either by the activity of canals connecting the harbor basins to the river (in freshwater-dominated harbor environments), or by the acceleration of deltaic progradation (on floodplains, coastal alluvial fans, paleo-channels, delta-fronts, and prodeltas) (Table 1).

Generally, these allochthonous particle fluxes are anti-correlated with the second source of sedimentary particles in harbor deposits, the biogenic fluxes (34%, Table 1). This negative correlation is due to the nature of these fluxes which are considered autochthonous as they are produced *in situ*. This is why this environmental variable is so predominant in the water columns of the harbor basins of Trajan and Ephesus (Table 1). The grouping of elements representative of biogenic fluxes (L.O.I., Ca, and Sr) is usually found on the axis of Factor 1, in a position opposite to that of the constituent elements of detrital fluxes. They are most often evidence for relatively calm hydrodynamic conditions as these favor the production of biomass, whether plant (organic matter) or carbonated (skeletal remains). While the production of biomass depends on paleo-geographic changes that in turn encourage

environments with weaker water currents (swamp, marine, enclosed harbor, peat, lagoon, epilimnic, brackish, or eutrophic), eutrophication and urban sewage inputs also participate effectively in the production of these biogenic fluxes.

In order of importance, authigenic fluxes (20%) are next; these correspond to the redox conditions of the environment. This environmental parameter expresses the conditions of the ventilation of the harbor water column, that is, its speed of renewal, which is rapid for well-oxygenated milieus (Mn, K, Ti, Zn, Cr, Co, Cd), and slow in environments deficient in oxygen (S, Mo, U, Pb, Ag, Cu). In the first case, deltaic progradation (on floodplains, freshwater-dominated harbors, coastal alluvial fans, paleo-channels, delta-fronts and prodeltas) and breaking of waves on the shore (on delta-fronts and beaches) are the principal processes of oxygenation identified. In the second case, the processes limiting the presence of dissolved oxygen in the harbor waters are peat formation arising from enclosing harbor basins, interflood periods, urban sewage inputs, and eutrophication (in enclosed harbors and peat bogs). The range of anoxic environments is relatively extensive, as we have identified marine, lagoon, marshy, peaty, and harbor environments. In terms of paleo-environmental reconstructions, this factor is particularly instructive for evaluating the degree to which the environments encountered are open; the more the milieu is open, the higher the proportion of dissolved oxygen, and vice versa.

The following factor, which can sometimes be intermixed with Factor 1, expresses the mineralogy and the lithology of the sediments (11%). This factor therefore characterizes rather well the granulometric distribution of the stratigraphic sequences studied, in which the fine sediments are dominated by alumino-silicates (Al, Ti, Mg, Rb, Ga, Li) and the coarsest by siliciclastic minerals (Zr, Th, REEs, Si). Besides this characteristic useful for reconstructing variations in the hydrodynamics of harbor currents, this environmental variable

445 also provides unique information on the geological sources of sediments from a given
446 watershed.

447 The fifth variable revealed by factor analysis represents the pollutants of anthropogenic
448 origin (10%) (Table 1). This component is made up of heavy metals (Pb, Cu, Sn, Ag, Cd)
449 which have been exploited by humans in various ways for millennia. However, it is necessary
450 to be cautious in using this factor because the precipitation and thus the enrichment of these
451 metallic trace elements depends on the intensity of human activity, but also on the physico-
452 chemical conditions (Delile et al., 2015) and the turbulence of the aquatic milieus (Delile et
453 al., 2017). In order to be free of these two environmental constraints that can bias the reading
454 of human influence over time, we normalize the trace elements of interest to an element
455 representative of the terrestrial crust (Al, Th, REEs, etc.) and calculate the enrichment factor
456 on the basis of representative crustal values specific to the local context in question. These are
457 easily obtainable from the pre-harbor levels of the studied sites.

458 The last factor of environmental control, which completes the total geochemical
459 variability in a given harbor deposit sequence, is the marine influence (10%) in the sediments
460 based on their enrichment in Na (Table 1). This factor is particularly useful when the absence
461 of microfauna renders reconstructions of paleo-environments difficult. Generally in the case
462 of a harbor milieu open to the sea, the increase in the proportion of seawater compared to
463 freshwater leads to the formation of a harbor milieu under marine influence (i.e., a marine-
464 dominated harbor). A large range of harbor facies depends on the degree of opening of the
465 harbor basin to the sea and its distance from the river mouth (if present). In contrast, an
466 increase in the values of this factor generally characterises pre-harbor levels of the delta front
467 type.

Once these environmental variables have been identified, combining their respective information enables determination of paleo-environments and the processes that produced them.

4.3. The sources of the Tiber river-mouth sediments inferred from Pb isotopes

Within the scope of previous studies focusing on lead pollution generated by Rome and trapped in (recorded by) its harbor basins during the Roman and medieval periods (Delile et al., 2014b, 2017), Pb isotope compositions were measured on four harbor sediment cores. In the following, we proceed with an in-depth study of the natural Pb isotopic signal to understand its meaning. Of the total of 177 samples analysed, 75 were considered uncontaminated (Figs. 5 et 6). The Pb isotopic compositions of these samples reflect the natural background of Pb in the waters of the Tiber whose characteristics are related to the geology of the Tiber River watershed.

In order to optimize the reading of the geological signal from the Pb isotopes, we converted the Pb isotope compositions into their corresponding geochemically informed parameters, which are the Pb model age T_{mod}, the $^{238}U/^{204}Pb$ (μ) and the $^{232}Th/^{238}U$ (κ) ratios (Fig. 5B) (Albarède et al., 2012). In short, T_{mod} (Ma = million years) is a proxy tracking the tectonic age of crystalline rocks and their associated ore deposits, and thus closely maps the distribution of the Alpine, Hercynian, and early Paleozoic provinces of Europe. Mu (μ) and kappa (κ) delineate collision belts or tectonically stable areas, and thus divide Europe into coherent regions (Blichert-Toft et al., 2016).

In Fig. 5, uncontaminated harbor sediments from Ostia Antica (core PO2) and Portus (cores TR14, CN1, and PTXI-3) include one main source of natural Pb labeled “component α” (Delile et al., 2014b, 2017). This natural component α consists of two sub-components α’ and α” connected by a mixing line (grey dotted line in Fig. 5). As recently demonstrated by Delile et al. (2014b, 2017), these uncontaminated sediments represent a mixture of two local

493 low-$^{204}Pb/^{206}Pb$ sources, reflecting the geology of the Tiber River watershed. One source is
494 the upstream, erodible recent Apennine limestones (component α"), which are very similar to
495 Pb dissolved in modern Mediterranean seawater (Stumpf et al., 2010), and the other is the
496 recent volcanic rocks of the Alban Hills (component α') (Conticelli et al., 2002; D'Antonio et
497 al., 1996). As mentioned in section 4.1.2., the elemental composition of the volcanic rocks of
498 the Alban Hills is similar to that of the RMP-LD. This geochemical homogeneity of the
499 volcanic districts located in the vicinity of the Tiber Delta (Colli Albani, Vulsini, Cimini,
500 Vicano, Ceriti, and Sabatini) is also observed for their Pb isotopic compositions (Conticelli et
501 al., 2007; Mattei et al., 2010). In other words, the Pb isotopic fingerprint of the Alban Hills
502 (component α') reflects that of the RMP-LD as a whole. Furthermore, in the trend α'−α"
503 uncontaminated sediments split distinctly into two groups according to their kappa values
504 (Fig. 5A) or $^{208}Pb/^{206}Pb$ ratio (Fig. 5B). The sandy pre-harbor sediments show high values,
505 while the harbor sediments dominated by clays and silts are characterized by lower values. It
506 thus appears that a particle size gradient can be inferred from the Pb isotopic compositions of
507 the sediments.

508 To test this linear relationship, we calculated two indices labeled *f*α' and *f*α" that
509 measure the proportion of the natural sub-components α' and α" in all uncontaminated
510 sediment samples (equation details in the Materials and Methods section of Delile et al.,
511 2017). In Fig. 6, where these index values are plotted against the sand, silt, and clay
512 percentages of the same samples, it is clear that the particle size distribution of the Tiber delta
513 sediments largely correlates with the proportions of the two main natural sedimentary sources
514 of the Tiber's watershed. On the one hand, sandy particles correlate positively with the
515 volcanic component (*f*α') (r = 0.69) and, on the other hand, fine particles correlate well with
516 the Apennine limestones (*f*α") (r = 0.68) (Fig. 6). Such a distinction is not unexpected, as the
517 changes in mineral sorting processes that result from varying levels of hydrodynamic activity

518 modify the mineralogy and thus the geochemistry of the transported sediments. According to
519 Garçon et al. (2014), a "heavy mineral effect" alters the Pb isotopic budget of both coarse and
520 fine fluvial sediments. Some heavy minerals concentrated in coarse sediments are extremely
521 radiogenic, allowing sandy sediments to grow in more radiogenic $^{208}Pb/^{206}Pb$ values (Garçon
522 et al., 2014) and, thereby, acquire elevated values of κ (r between $^{208}Pb/^{206}Pb$ vs $\kappa \sim 0.7$). The
523 sandy deposits of the Tiber delta's littoral facies are strongly enriched in heavy minerals
524 (Belfiore et al., 1987) that take the form of placers (Salomon, 2013) (Fig. S3) derived from
525 the erosion of the Monti Sabatini or the Colli Albani (Funiciello, 1995; Ventriglia, 1971). The
526 presence of such minerals requires a source close to the deposit area (Carling and Breakspear,
527 2006), located less than 20 km away according to Thomas and Thorp (1993).

528 A primarily volcanic origin for the sandy particles of the Tiber delta, which would have
529 derived from erosion of the volcanic rocks in the Alban Hills, but also from the other volcanic
530 districts that are part of the RMP-LD surrounding the Tiber delta (Vulsini, Cimini, Vicano,
531 Ceriti, and Sabatini), is reinforced by a particularly significant correlation coefficient between
532 F1 and *fα'* measured in core PO2 (r = -0.7).

533 *4.4. Chronology of the life cycle of the harbor*

534 According to the present sedimentological, geochemical, and Pb isotopic results, the
535 paleo-environmental evolution of the water column of Rome's first harbor took place in five
536 stages (gray and white bands in Fig. 4B) as described further below. First, however the
537 chronostratigraphic framework of the PO2 core will be discussed.

538 *4.4.1. Comments on the chronostratigraphic model of the PO2 core*

539 The S-shape of the ^{14}C age-depth model obtained for the PO2 core (Fig. 2) testifies to a
540 well-known and well-documented phenomenon in harbor geoarcheology resulting from
541 multiple dredging operations. These practices, observed in many ancient Mediterranean

harbor basins, consist in removing part of the sedimentary thickness of the harbor deposits in order to preserve a sufficiently deep draught to guarantee the circulation of ships and thus maintain the operation of the port. This phenomenon is generally detected on the basis of (1) sharp drops in apparent sedimentation rates and (2) chronological inversions due to removal and mixing of part of the harbor deposits (Marriner and Morhange, 2006). At Ostia, such dredging markers have been identified several times and have been the subject of specific studies by Salomon et al. (2016) and Goiran et al. (2017). To sum up these studies, the chronostratigraphic model of the ancient port basin of Ostia contains four chronological gaps reflecting three potential dredging phases. These gaps are distributed as follows (red stars in Fig. 2):

Gap 1 is identified by a sharp drop in sedimentation rate between the last date from unit A at 1050 cm depth (835-736 BC) and the first date from unit B1 at ~ 870 cm depth (358-113 BC). This chronological gap either testifies to the excavation of the harbor basin of Ostia or to a later dredging phase that occurred around the middle of the 4th c. BC.

Gap 2 is identified by a chronological inversion recorded at 815 cm depth (728-265 BC) reflecting the mixing of part of the harbor deposits where older deposits are mixed in with younger deposits. Since this date lies within the chronological ranges of the sedimentary units A and B, this older date may refer to the same dredging event described above. Another explanation could be that this date, which is based on terrestrial material (charcoal), was part of reworked material coming from the Tiber.

Gap 3 is identified by a sharp drop in the sedimentation rate between the last date of unit B1 at ~ 585 cm depth (387-204 BC) and the first date from unit B2 at 526 cm depth (163 BC-AD 16). This chronological gap reflects a second potential dredging phase that took place at the earliest before the mid-2nd c. BC.

566 **Gap 4** is identified by a last sharp drop in the sedimentation rate between the date at 378 cm
567 depth (158 BC-AD 24) and that at ~ 550 cm depth (AD 80-231). This chronological gap
568 reflects a third and last potential dredging phase that took place at the latest during the 1st c.
569 AD.

570 *4.4.2. The pre-harbor environment*

571 The pre-harbor unit A is composed of bedded and shelly grey sands with *Posidonia,*
572 attesting to a depositional environment of deltaic progradation. According to the age-depth
573 model of the core (Fig. 2), this unit dates from the early 1st millennium (modeled dates are
574 situated between the end of the 9th c. and the early 8th c. BC) to the middle of the 4th c. BC
575 (Goiran et al., 2014, 2017; Delile et al., 2017). Figure 4 shows a relatively high-energy
576 environment revealed by the negative values of Factor 1, faithfully reporting the rather coarse
577 grain size of this unit (Fig. 2). The main geochemical aspects of this unit are the high salinity
578 (high Na, F4 in Fig. 4B) and the oxygen depletion (negative values of the Factor 3 in Fig. 4B),
579 consistent with the marine-to-brackish lagoonal ostracod groups observed by Goiran et al.
580 (2014). Also reported in this work are freshwater inflows (Fig. 2) that explain the turbulent
581 conditions attested to by the siliciclastic flux (Factor F1). While the main mineralogical and
582 geochemical characteristics of these pre-harbor deposits are like those recorded at *Portus*
583 (Delile et al., 2014a), the freshwater influence on the site of the ancient harbor basin of Ostia
584 Antica strengthens the hypothesis of the presence of an estuarine river mouth, whose fluvial
585 sand inputs were remobilized by the marine swell. Due to the continuity and regularity of the
586 seawater influence during almost five centuries, as well as the dramatic oxygen depletion (F3
587 negative values in Fig. 4) and the freshwater influence, it is difficult to posit this pre-harbor
588 deposit as a credible "tsunami event I" as has been postulated between 800 BC and 400 BC by
589 Hadler et al. (2015a). In the somewhat more realistic and less catastrophic perspective taken
590 here, the assemblage of observed and measured faunal, sedimentological, and geochemical

indicators rather converge towards a pre-harbor deposit typical of a classic deltaic front sequence, which is well recorded both at the scale of the site itself and of the Tiber delta as a whole (Mazzini et al., 2011; Goiran et al., 2012; 2014; Salomon, 2013; Salomon et al., 2012, 2018; Delile et al., 2014a; Sadori et al., 2016)

4.4.3. The lower harbor sequence

From the middle of the 4th c. to the beginning of the 2nd c. BC, the environmental conditions change markedly towards a quiet milieu between -9 and -5.7 m *b.g.l.* (i.e., between 6.6 and 3.3 m *b.p.s.l.* or between 5.8 and 2.5 m *b.a.s.l.*) (Fig. 4), as suggested by the compact dark grey silt deposits (Goiran et al., 2012, 2014, 2017; Sadori et al., 2016). Classically, this unit B1 resulted from the creation of the harbor basin of Ostia Antica, a typical well-protected harbor, still connected to fluvial-marine environments. The significant reduction of the hydrodynamic conditions of the currents leading to the deposit of unit B1 is clearly indicated by Factor 1, which shows a drastic decrease in siliciclastic fluxes (Fig. 4B). Inversely, the same process led to an increase in the proportion of fine particles in the deposit as seen in the positive values of Factor 2 (aluminosilicate flux in Fig. 4B). The third geochemical characteristic of unit B1 is the distinction of two regimes in the paleo-environmental dynamics of the harbor water column. Based on the seawater influence (Factor 4 in Fig. 4B), unit B1 can be divided into two subunits:

- Subunit B1a (from -9 to -7 m *b.g.l.*; i.e., between 6.6 and 4.6 m *b.p.s.l.* or between 5.8 and 3.8 m *b.a.s.l.*) reflects a marine-dominated regime since the F4 values (seawater influence) always remain positive, although being lower than those of unit A due to the connection of the harbor basin to the Tiber river;

- Subunit B1b (from -7 to -5.7 m *b.g.l.*; i.e., between 4.6 and 3.3 m *b.p.s.l.* or between 3.8 and 2.5 m *b.a.s.l.*) reflects a freshwater-dominated regime since the F4 values (seawater

615 influence) are negative. This is corroborated by the ostracodal freshwater group in this
616 subunit (Fig. 2).

617 According to the ^{14}C age-depth model of the PO2 core (Fig. 2A), the passage from
618 subunit B1a to B1b took place around the middle of the 3rd c. BC. This change in the paleo-
619 environmental dynamics of the harbor water column at this particular time is not surprising,
620 and even rather consistent with the known progradation phases of the Tiber river delta.
621 Giraudi et al. (2009), Bicket et al. (2009), Giraudi (2011), and Salomon et al. (2018) recorded
622 intense Tiber delta progradation between the 4th c. BC and the 5th c. AD which began after a
623 sudden paleo-geographic event. Indeed, a major step of the Tiber delta construction occurred
624 between the 8th and the 3rd c. BC due to the sharp southward migration of the river mouth, in
625 the direction of the harbor basin of Ostia (Bellotti et al., 2011; Milli et al., 2013; Salomon et
626 al., 2018). Over this time period, the rate of the progradation of the river mouth is estimated to
627 be around 5-6 m/year (Milli et al., 2013). According to Milli et al. (2013) a strong Tiber flood
628 event that occurred during the climate cooling phase of the Iron Age (Bond cycle B2, Bond et
629 al., 1997, 2001) probably led to the shift of the Tiber mouth location. In this new paleo-
630 geographical context of the Tiber delta, the increasing fluvial inputs into the harbor basin of
631 Ostia Antica between the 4th and the 2nd centuries BC (the chronological range of unit B1)
632 caused the paleo-environmental dynamic change of the harbor water column towards a
633 freshwater-dominated regime in about the early 3rd c. BC.

634 This gradual and continuous increase of the freshwater influence in the harbor muds is
635 not consistent with the surge of a tsunami deposit in the “lagoonal harbour” which is referred
636 to as “event II” by Hadler et al. (2015a). Such a “high-energy event layer” should present a
637 sudden break and a sustainable return of seawater influence in this deposit, and not the
638 reverse.

639 *4.4.4. The upper harbor sequence*

Between the 2nd c. BC and the 3rd c. AD, a new harbor sequence called unit B2 became established at a depth of between 5.7 and 3.2 m *b.g.l.* (i.e., between 3.3 and 0.8 m *b.p.s.l.* or between 2.5 and 0 m *b.a.s.l.*; Figs. 2 and 4). This unit presents sedimentological and geochemical characteristics that are different from the lower harbor sequence as the deposit of coarse sands (Fig. 2) led to a retreat of aluminosilicate minerals (negative values of Factor 2) in favor of siliciclastic particles (negative values of Factor 1). In unit B2, three major pulses of siliciclastic flux reflect periods of strong hydrodynamic currents in the harbor basin; they are evidence of high-energy floods of the Tiber (Goiran et al., 2014, 2017, Salomon et al., 2016). These phases were followed by periods of relatively calm currents in which anoxic conditions were established (negative values of Factor 3 in Fig. 4B). Finally, unit B2 reflects infilling of the harbor basin, which appears to have been subject to the hydrological rhythms of the Tiber. During periods of major inundations, the currents renewed the oxygenation of the water masses, while in periods of low water level, the less energetic currents led to the development of anaerobic conditions.

According to Hadler et al. (2015a) and Wunderlich et al. (2018) unit B2 would incorporate yet a third tsunami event dated to between AD 1 and 50. As speculated above for their second tsunami event, our geochemical analyses should show a sudden break illustrating a sustainable return of seawater influence in this deposit. However, exactly the opposite is recorded, since the influence of seawater is becoming increasingly absent in unit B2 (Fig. 4B). Moreover, the occurrence of a tsunami would have been observed at different places in the delta, such as the Ostia lagoon (Bellotti et al., 2011; Vittori et al., 2015) and the Maccarese lagoon (Bellotti et al., 1994, 2007; Giraudi, 2002, 2004, 2011; Di Rita et al., 2010; Jouannic et al., 2013), since the sediment-transport distances for tsunamis vary from several hundred meters to a few kilometres from the shore (a regional signature) (Minoura et al., 1997; Gelfenbaum and Jaffe, 2003; Morton et al., 2007). However, none of the studies carried out

665 on the sedimentary deposits of the Tiber delta have mentioned any such event. This is not
666 surprising as the three high-energy events of tsunamigenic origin were recorded in a single
667 core (core OST 3), among eight cores taken by Hadler et al. (2015a). Thus the tsunamigenic
668 fingerprint appears to be local rather than regional. However, as pointed out by Sadori et al.
669 (2016), if such a catastrophic event had taken place during the 1st c. AD, no doubt it would
670 have been recorded by Roman historians, who paid close attention to natural phenomena; this
671 is, however, not the case. Rather than assuming a scenario including a third tsunami event as
672 speculated by Hadler et al., (2015a), we present below in three steps using an integrated
673 approach (i.e. combined hydro-climatic, historical, and sedimentological and geochemical
674 data) an alternative scenario that takes into account the environmental context of this period.

675 (i) During the time period covered by unit B2 (2nd c. BC to 3rd c. AD), a major hydro-
676 sedimentary event, which is characterized by an increase in the frequency of floods, occurred
677 during the period of the 1st c. BC to the 2nd c. AD approximately at several places in the
678 western Mediterranean region (Berger and Bravard, 2012). Based on the flood events of the
679 Tiber River in Rome recorded by Bersani and Bencivenga (2001), corroborating the work of
680 Le Gall (1953), such an increase in the flood frequency of the Tiber took place between
681 approximately the 2nd c. BC and the 2nd c. AD.

682 (ii) During this major hydro-sedimentary crisis, several coastal sites experienced an
683 acceleration of deltaic progradation on the Mediterranean coast due to the erosion and
684 transport of substantial amounts of sedimentary loads. This was the case for the Rhône delta
685 between the 1st c. BC and the end of the 2nd c. AD (Arnaud-Fasseta, 2000, 2002), the Argens
686 delta in eastern Provence (Excoffon et al., 2010, 2016) and the Küçük Menderes delta in
687 Turkey from the 2nd c. BC to the 1st c. AD at least (Delile et al., 2015). In the case of the Tiber
688 delta, the work of Giraudi et al. (2009) distinctly shows an acceleration phase of progradation
689 that occurred between the 3rd c. BC and the 3rd c. AD.

690 (iii) This rapid progression of the progradation of the deltas stimulated by a sporadic
691 deterioration of hydro-climatic conditions brought on the accelerated siltation of numerous
692 harbor basins in the Mediterranean such as that of the great Roman harbor of Narbonne in the
693 1st c. (Rescanières, 2002), and those of Frejus (Excoffon et al., 2010), Ephesus (Delile, 2014;
694 Delile et al., 2015), Naples (Delile et al., 2016a), Pisa (Benvenuti et al., 2006; Mariotti Lippi
695 et al., 2007), as well as that of Trajan at *Portus* (Delile et al., 2014a). For all these reasons, we
696 consider that at this period the acceleration of the deltaic progradation of the Tiber, partly
697 controlled by climate, but partly also by humans, moved the river mouth of the Tiber even
698 further downriver, and thus even further from the harbor basin (Fig. 2), on the one hand, and
699 mechanically caused an aggradation of the alluvial floor, on the other hand. This process thus
700 favored the evacuation of the strongest floodwaters accompanied by their sands in the harbor
701 basin of Ostia Antica. This scenario also emphasises the importance of consulting
702 contemporary sources such as the Roman author Strabo (64-58 BC / AD 21-25), who wrote:
703 "Ostia had the inability to maintain or consider a convenient sheltered harbor due to the
704 amount of Tiber sediments transported down to the seashore" (Geography, 5, 3, 5, translated
705 by H. L. Jones).

706 *4.4.5. The abandonment of the harbor basin*

707 The yellow bedded silts of unit C (Figs. 2 and 4) from the 3rd c. AD onward represent
708 floodplain deposits which definitively isolated the harbor basin from the sea. Unit C presents
709 the same geochemical characteristics as the floodplain deposits recorded in the uppermost unit
710 (unit C) of the Trajan basin at *Portus* (Delile et al., 2014a). In both cases, the depositional
711 environment was freshwater (negative values of F4), oxygenated conditions prevailed
712 (constant positive values of F3), and the detrital particles dominated by the aluminosilicate
713 minerals demonstrate the fineness of these sediments (high positive values of F2 and F1) (Fig.

4). These characteristics indicate that the abandoned harbor had finally been overrun by the floodplain around five centuries before the harbor of Trajan suffered the same fate.

This abandonment phase of the harbor basin appears to have been mistaken with the establishment of a fluvial harbor (Hadler et al., 2015) called the “younger fluvial harbour phase” in Wunderlich et al. (2018). Indeed, these authors argue for a shift from a harbor of lagoon type towards a fluvial harbor phase (or “harbour generation II”) located between - 0.5 and - 1 m *b.p.s.l.* (see Fig. 7 in Hadler et al., 2015), that is to say between - 0.2 m *b.a.s.l* and + 0.3 m *above a.s.l.* These values, inferred from the ancient biological sea level dated to AD 230-450 by Goiran et al. (2009), show unambiguously that the water column disappears at these depths because the environment became terrestrial. Consequently, the establishment of a river harbor at these depths is strictly impossible. For this reason, we strongly suggest using ancient sea levels to characterize harbor levels and phases rather than the simple measurement of present sea level.

5. Conclusions

The 3000-year-old geochemical record preserved in the sediment core from the ancient harbor basin of Ostia Antica located in the Tiber delta has provided new insights into some of the aquatic paleo-environmental conditions, insights that had not been gleaned by the "classical" proxies used in the geoarcheological studies carried out in this harbor basin thus far. Associated with factor analysis, elemental geochemistry applied at high resolution to some forty chemical elements has enabled discrimination of the main environmental factors leading to the formation of the harbor basin deposits, classified in order of importance as (i) strong hydrodynamics (i.e., high-velocity currents) (the siliciclastic terrigenous signal ~ 47%), (ii) quiet hydrodynamics (the aluminosilicate terrigenous signal ~ 13%), (iii) water column

738 ventilation (the authigenic fluxes ~ 10%), and (iv) seawater vs. freshwater influence (~ 7%).
739 A first comparison of these environmental variables affecting the harbor water column at
740 Ostia Antica with those identified using the same method in the ancient harbors of Trajan and
741 Claudius (*Portus*), as well as those of Ephesus and Naples, has shown that the formation of
742 the harbor basin deposits took place by means of similar geochemical fluxes, whose
743 respective weights were relatively constant from one harbor basin to the other. This
744 observation is not surprising as all these harbor sites, except for that of Naples (situated in a
745 small coastal bay north of the gulf of Naples) are located on deltas. Thus the paleo-
746 environmental evolution of the water column of the harbor basins was conditioned by the
747 coastal geomorphology of the sites where the harbors were established.
748 By focusing on sediments uncontaminated by anthropogenic lead, the study of Pb
749 isotopes has shown that it is possible to both identify the geological sources of sedimentary
750 particles of the Tiber delta and distinguish the fine from the coarser particles. The particle size
751 distribution of the Tiber delta sediments largely correlates with the proportion of the two main
752 natural sedimentary sources of the Tiber's watershed: The sandy particles correlate positively
753 with the volcanic rocks, while the fine particles are subject to rough correlations with the
754 Apennine limestones.
755 The present study also sheds new light on the chronology of the life cycle of the harbor
756 at Ostia Antica. First, the Na enrichment of pre-harbor level sediments, indicating, as at
757 *Portus*, an environment dominated by marine influence, remained when the harbor basin was
758 dug out around the middle of the 4th century BC, but to a lesser degree. Then, starting around
759 the 3rd c. BC, the initial marine-dominated regime of the harbor basin shifted towards a
760 freshwater-dominated milieu due in part to intense Tiber delta progradation caused by a short
761 phase of climate deterioration, and due in part to human action. This influence of Tiber waters
762 in the water column of the harbor basin reached a threshold of no return between the 2nd c. BC

763 and the 3rd c. AD because the harbor basin was affected by the high-energy floods of the Tiber
764 river. During this period, the geochemical signal of the coarse harbor deposits carefully
765 recorded the hydrological rhythms of the Tiber, marked by the alternation of major inundation
766 phases and pronounced low-water phases. Again during this period a phase of increased
767 progradation of the Tiber delta occurred, resulting from an increase in the flood frequency of
768 the Tiber between approximately the 2nd c. BC and the 2nd c. AD. While Hadler et al. (2015a)
769 and Wunderlich et al. (2018) have advocated for a high-energy event to interpret the coarsest
770 B2 unit, our geochemical data are more consistent with the scenario proposed by Goiran et al.
771 (2014), Sadori et al. (2016) and Salomon et al. (2016) who call on an upsurge in the frequency
772 of floods, which carried the sands into the harbor basin of Ostia Antica that led to its
773 abandonment. This final phase of abandonment cannot be replaced by a river port
774 environment, as argued by Hadler et al. (2015a) and Wunderlich et al. (2018), since these
775 deposits are located in part above ancient sea level (- 0.2 to + 0.3 m *b.a.s.l.*); the harbor water
776 column no longer existed at that time.
777 Finally, this study has also provided the opportunity to test the hypothesis of Hadler et
778 al. (2015a) that argues for three high-energy events ascribed to a tsunamigenic origin, which
779 would have thrice greatly affected the harbor basin of Ostia Antica. There are many
780 arguments against this hypothesis, whether historical (absence of historical accounts of such
781 events), geomorphological (inappropriate morphology of the coastline south of the Tiber
782 River mouth), stratigraphic (no traces of tsunami deposits in the area) (Sadori et al., 2016), or
783 anthropic (highest Pb abundances (anthropic contamination) recorded in the deposits of the
784 most recent so-called tsunami) (Delile et al., 2017). While the earliest tsunami appears to have
785 been mistaken for a classic deltaic front sequence of the Tiber, the other two high-energy
786 layers should record a sudden change to a sustainable return of seawater influence in these

deposits. However, our multi-elemental geochemical signal records the exact opposite, a strong freshwater component that increases towards the top of the stratigraphy.

Acknowledgments

We thank the Soprintendenza Speciale per i Beni Archeologici di Roma e Sede di Ostia for the authorization to access the area suspected to have hosted the ancient harbor basin of Ostia Antica in which the PO2 core was drilled. We are grateful to Philippe Telouk for ensuring that the mass spectrometers were always working well. We further acknowledge the ARTEMIS-SHS program and radiocarbon laboratory of Lyon for carrying out the radiocarbon dating. The Young Scientist Program of the Agence Nationale de la Recherche (CNRS) (ANR 2011 JSH3 002 01), the Roman Mediterranean Ports program (ERC grant agreement n° 339123), and the Ecole Française de Rome provided financial and logistical support. We finally thank the Editor, Neil Roberts, as well as two anonymous reviewers for their constructive comments which helped improve the manuscript, and Duncan Keenan-Jones for checking the English.

References

Albarède, F., Desaulty, A.-M., Blichert-Toft, J., 2012. A geological perspective on the use of Pb isotopes in Archaeometry. Archaeometry 54, 853–867.

Albarède, F., Telouk, P., Blichert-Toft, J., Boyet, M., Agranier, A., Nelson, B., 2004. Precise and accurate isotopic measurements using multiple-collector ICPMS. Geochimica et Cosmochimica Acta 68, 2725–2744.

Arnaud-Fassetta, G., 2000. Quatre mille ans d'histoire hydrologique dans le delta du Rhône. De l'âge du Bronze au siècle du nucléaire, Mémoires et documents de l'UMR PRODIG. Paris.

Arnoldus-Huyzendveld, A., 2005. The natural environment of the Agro Portuense, in: Portus, an Archaeological Survey of the Port of Imperial Rome, Archaeological Monographs of the British School at Rome 15. BSR, London, pp. 14–30.

Balland, A., 1965. Nova Urbs et « neapolis ». Remarques sur les projets urbanistiques de Néron. mefr 77, 349–393.

Belfiore, A., Bellotti, P., Carboni, M.G., Chiari, R., Evangelista, S., Tortora, P., Valeri, P.,

1987. Il delta del Tevere; le facies sedimentarie della conoide sommersa; Un' analisi statistica dei caratteri tessiturali, microfaunistici e mineralogici. Bollettino della Societa Geologica Italiana 106, 425–445.
Bellotti, P., Calderoni, G., Carboni, M.G., Di Bella, L., Tortora, P., Valeri, P., Zernitskaya, V., 2007. Late Quaternary landscape evolution of the Tiber River delta plain (Central Italy): new evidence from pollen data, biostratigraphy and 14C dating. Zeitschrift für Geomorphologie 51, 505–534.
Bellotti, P., Calderoni, G., Rita, F.D., D'Orefice, M., D'Amico, C., Esu, D., Magri, D., Martinez, M.P., Tortora, P., Valeri, P., 2011. The Tiber river delta plain (central Italy): Coastal evolution and implications for the ancient Ostia Roman settlement. The Holocene 21, 1105– 1116.
Bellotti, P., Chiocci, F.L., Milli, S., Tortora, P., Valeri, P., 1994. Sequence stratigraphy and depositional setting of the Tiber Delta; integration of high-resolution seismics, well logs, and archeological data. Journal of Sedimentary Research 64, 416–432.
Bellotti, P., Milli, S., Tortora, P., Valeri, P., 1995. Physical stratigraphy and sedimentology of the Late Pleistocene-Holocene Tiber Delta depositional sequence. Sedimentology 42, 617–634.
Benvenuti, M., Mariotti-Lippi, M., Pallecchi, P., Sagri, M., 2006. Late-Holocene catastrophic floods in the terminal Arno River (Pisa, Central Italy) from the story of a Roman riverine harbour. The Holocene 16, 863–876.
Berger, J.-F., Bravard, J.-P., 2012. Le développement économique romain face à la crise environnementale : le cas de la Gaule narbonnaisaise, in: Des Climats et Des Hommes. Berger, J.-F., Paris, pp. 269–289.
Bersani, P., Benvivenga, M., 2001. Le piene del Tevere a Roma dal V secolo a.C. all'ano 2000 (Servizio idrografico e mareografico nazionale). Dipartimento per i Servizi Tecnici Nazionali, Roma.
Bicket, A.R., Rendell, H.M., Claridge, A., Rose, P., Andrews, J., Brown, F.S.J., 2009. A multiscale geoarchaeological approach from the Laurentine shore (Castelporziano, Lazio, Italy). Géomorphologie : relief, processus, environnement 15, 241–256.
Blaauw, M., 2010. Methods and code for 'classical' age-modelling of radiocarbon sequences. Quaternary Geochronology 5, 512–518.
Blichert-Toft, J., Delile, H., Lee, C.-T., Stos-Gale, Z., Billström, K., Andersen, T., Hannu, H., Albarede, F., 2016. Large-scale tectonic cycles in Europe revealed by distinct Pb isotope provinces. Geochemistry Geophysics Geosystems 17, 3854–3864.
Bond, G., Kromer, B., Beer, J., Muscheler, R., Evans, M.N., Showers, W., Hoffmann, S., Lotti-Bond, R., Hajdas, I., Bonani, G., 2001. Persistent Solar Influence on North Atlantic Climate During the Holocene. Science 294, 2130–2136.
Bond, G., Showers, W., Cheseby, M., Lotti, R., Almasi, P., deMenocal, P., Priore, P., Cullen, H., Hajdas, I., Bonani, G., 1997. A Pervasive Millennial-Scale Cycle in North Atlantic Holocene and Glacial Climates. Science 278, 1257–1266.
Boyle, J.-F., 2002. Inorganic geochemical methods in paleolimnology, in: Tracking Environmental Change Using Lake Sediments: Physical and Geochemical Methods. Last WM, Smol JP, Berlin, pp. 83–141.
Bravard, J.-P., 2009. La géologie: les sciences de la Terre appliquées à l'archéologie, Archéologiques. Errance, Paris.
Carling, P.A., Breakspear, R.M.D., 2006. Placer formation in gravel-bedded rivers: A review. Ore Geology Reviews, Special Issue on Placer Formation and Placer MineralsSelected Papers presented at the 26th International Sedimentological Congress, Rand Afrikaans University, South Africa, 8 -- 12 July, 2002 28, 377–401.
Coarelli, F., 1988. I santuari, il Fiume, gli Empori, in: Storia Di Roma. Momigliano, A.,

Schiavone, A., Turin, pp. 127–152.
Conticelli, S., D'Antonio, M., Pinarelli, L., Civetta, L., 2002. Source contamination and mantle heterogeneity in the genesis of Italian potassic and ultrapotassic volcanic rocks: Sr–Nd–Pb isotope data from Roman Province and Southern Tuscany. Mineralogy and Petrology 74, 189–222.
Conticelli, S., Carlson, R.W., Widom, E., Serri, G., 2007. Chemical and isotopic composition (Os, Pb, Nd, and Sr) of Neogene to Quaternary calc-alkalic, shoshonitic, and ultrapotassic mafic rocks from the Italian peninsula: Inferences on the nature of their mantle sources, in: Cenozoic Volcanism in the Mediterranean Area. Beccaluva, L., Bianchini, G. & Wilson, M., pp. 171–202.
Croudace, I.W., Rothwell, R.G. (Eds.), 2015. Micro-XRF Studies of Sediment Cores, Springer. ed, Developments in Paleoenvironmental Research.
Cubizolle, H., 2009. Paléo-environnements, Collection U. Géographie. A. Colin, Paris, France.
D'Antonio, M., Tilton, G.R., Civetta, L., 1996. Petrogenesis of Italian Alkaline Lavas Deduced from Pb-Sr-Nd Isotope Relationships, in: Basu, A., Hart, S. (Eds.), Earth Processes: Reading the Isotopic Code, Geophysical Monograph. Basu, A., Hart, S., Washington, D.C., pp. 253–267.
De Vos, W., Tarvainen, T. (Eds.), 2006. Geochemical atlas of Europe. Part 2, Interpretation of geochemical maps, additional tables, figures, maps and related publications. Geological Survey of Finland, Espoo, Finlande.
Delile, H., 2014. Signatures des paléo-pollutions et des paléoenvironnements dans les archives sédimentaires des ports antiques de Rome et d'Éphèse (Doctorat de géographie / géoarchéologie). Université Lumière Lyon 2, Lyon.
Delile, H., Mazzini, I., Blichert-Toft, J., Goiran, J.-P., Arnaud-Godet, F., Salomon, F., Albarède, F., 2014a. Geochemical investigation of a sediment core from the Trajan basin at Portus, the harbor of ancient Rome. Quaternary Science Reviews 87, 34–45.
Delile, H., Blichert-Toft, J., Goiran, J.-P., Keay, S., Albarède, F., 2014b. Lead in ancient Rome's city waters. PNAS 111, 6594–6599.
Delile, H., Blichert-Toft, J., Goiran, J.-P., Stock, F., Arnaud-Godet, F., Bravard, J.-P., Brückner, H., Albarède, F., 2015. Demise of a harbor: A geochemical chronicle from Ephesus. Journal of Archaeological Science 53, 202–213.
Delile, H., Goiran, J.-P., Blichert-Toft, J., Arnaud-Godet, F., Romano, P., Bravard, J.-P., 2016a. A geochemical and sedimentological perspective of the life cycle of Neapolis harbor (Naples, southern Italy). Quaternary Science Reviews 150, 84–97.
Delile, H., Keenan-Jones, D., Blichert-Toft, J., Goiran, J.-P., Arnaud-Godet, F., Romano, P., Albarède, F., 2016b. A lead isotope perspective on urban development in ancient Naples. PNAS 113, 6148–6153.
Delile, H., Keenan-Jones, D., Blichert-Toft, J., Goiran, J.-P., Arnaud-Godet, F., Albarede, F., 2017. Rome's urban history inferred from Pb-contaminated waters trapped in its ancient harbor basins. Proceedings of the National Academy of Sciences 114, 10059–10064.
Domergue, C., Rico, C., 2014. Les itinéraires du commerce du cuivre et du plomb hispaniques à l'époque romaine dans le monde méditerranéen. Presented at the La Corse et le monde méditerranéen des origines au moyen-âge : échanges et circuits commerciaux, BSSHNC, Bastia, pp. 135–168.
Eisele, J., Abouchami, W., Galer, S.J.G., Hofmann, A.W., 2003. The 320 kyr Pb isotope evolution of Mauna Kea lavas recorded in the HSDP-2 drill core. Geochemistry, Geophysics, Geosystems 4, 1–32.
Excoffon, P., Bonnet, S., 2016. Restitution de la morphologie littorale et aménagements

portuaires à Forum Iulii, in: Les Ports Dans l'espace Méditerranéen Antique. Sanchez, C. and Jezegou, M.-P., Montpellier, pp. 339–352.
Excoffon, P., Bonnet, S., Devillers, B., Berger, J.-F., 2010. L'évolution du trait de côte aux abords de Fréjus de sa fondation jusqu'à la fin du 1er s. ap. J.-C., in: Archéologie Des Rivages Méditerranéens : 50 Ans de Recherche. Delestre, X., pp. 47–53.
Finkler, C., Fischer, P., Baika, K., Rigakou, D., Metallinou, G., Hadler, H., Vött, A., 2018. Tracing the Alkinoos Harbor of ancient Kerkyra, Greece, and reconstructing its paleotsunami history. Geoarchaeology 33, 24-42.
Funiciello, R. (Ed.), 1995. La geologia di Roma: il centro storico. Istituto poligrafico e Zecca dello Stato, Roma, Italie.
Garçon, M., Chauvel, C., France-Lanord, C., Limonta, M., Garzanti, E., 2014. Which minerals control the Nd–Hf–Sr–Pb isotopic compositions of river sediments? Chemical Geology 364, 42–55.
Gelfenbaum, G., Jaffe, B., 2003. Erosion and Sedimentation from the 17 July, 1998 Papua New Guinea Tsunami. Pure appl. geophys. 160, 1969–1999.
Giaime, M., Morhange, C., Carayon, N., Flaux, C., Marriner, N., 2016. Les ports antiques des petites îles de Méditerranée. Proposition d'une typologie géoarchéologique, in: Géoarchéologie Des Îles de Méditerranée. Paris, pp. 165–176.
Giraudi, C., 2011. The sediments of the 'Stagno di Maccarese' marsh (Tiber river delta, central Italy): A late-Holocene record of natural and human-induced environmental changes. The Holocene 21, 1233–1243.
Giraudi, C., 2002. Evoluzione ambientale tardo-olocenica nell'area comprente il sto eneolitico di Maccarese (Fiumicino), in: Le Dune, Il Lago, Il Mare. Una Communita Di Villaggio Dell'Eta Del Rame a Maccarese. Manfredini, A., Firenze, pp. 25–35.
Giraudi, C., 2004. Evoluzione tardo-olocenica del delta del Tevere. Il Quaternario Italian Journal of Quaternary Science 17, 477–492.
Giraudi, C., Tata, C., Paroli, L., 2009. Late Holocene evolution of Tiber river delta and geoarchaeology of Claudius and Trajan Harbor, Rome. Geoarchaeology 24, 371–382.
Goiran, J.-P., Morhange, C., 2003. Géoarchéologie des ports antiques en Méditerranée : problématiques et études de cas, in: Topoi. pp. 647–669.
Goiran, J.-P., Salomon, F., Mazzini, I., Bravard, J.-P., Pleuger, E., Vittori, C., Boetto, G., Christiansen, J., Arnaud, P., Pellegrino, A., Pepe, C., Sadori, L., 2014. Geoarchaeology confirms location of the ancient harbour basin of Ostia (Italy). Journal of Archaeological Science 41, 389–398.
Goiran, J.-P., Salomon, F., Pleuger, E., Vittori, C., Mazzini, I., Boetto, G., Arnaud, P., Pellegrino, A., 2012. Port antique d'Ostie. Chronique des activités archéologiques de l'École française de Rome 123, 1–7.
Goiran, J.-P., Salomon, F., Vittori, C., Delile, H., Christiansen, J., Oberlin, C., Boetto, G., Arnaud, P., Mazzini, I., Sadori, L., Poccardi, G., Pellegrino, A., 2017. High chrono-stratigraphal resolution of the harbour sequence of Ostia: palaeo-depth of the bassin, ship drought & dredging, in: Fluvial Landscapes in the Roman World: Rivers and Their Influences on Roman Life, Journal of Roman Archaeology: Supplementary Series. T. Franconi, Portsmouth, pp. 67–83.
Goiran, J.-P., Tronchère, H., Collalelli, U., Salomon, F., Djerbi, H., 2009. Découverte d'un niveau marin biologique sur les quais de Portus : le port antique de Rome. Méditerranée 112, 59–67.
Hadler, H., Vött, A., Fischer, P., Ludwig, S., Heinzelmann, M., Rohn, C., 2015a. Temple-complex post-dates tsunami deposits found in the ancient harbour basin of Ostia (Rome, Italy). Journal of Archaeological Science 61, 78–89.
Hadler, H., Baika, K., Pakkanen, J., Evangelistis, D., Emde, K., Fischer, P., Ntageretzis, K.,

967 Röbke, B., Willershäuser, T., Vött, A., 2015b. Palaeotsunami impact on the ancient
968 harbour site Kyllini (western Peloponnese, Greece) based on a geomorphological
969 multi-proxy approach. Zeitschrift für Geomorphologie, Supplementbände 7–41.
970 Hesnard, A., 1994. Une nouvelle fouille du port de Marseille, Place Jules Verne. Comptes
971 rendus de l'Académie des Inscriptions et Belles-Lettres 1, 195–216.
972 Iadanza, C., Napolitani, F., 2006. Sediment transport time series in the Tiber River. Physics
973 and Chemistry of the Earth 31, 1212–1227.
974 Jouannic, G., Gillot, P.-Y., Goiran, J.-P., Lefevre, J.-C., Siani, G., Salomon, F., Arnoldu-
975 Huyzendveld, A., 2013. Tephrochronological study in the Maccarese lagoon (near
976 Rome, Italy): identification of Holocene tephra layers. Quaternaire. Revue de
977 l'Association française pour l'étude du Quaternaire 24, 65–74.
978 Keay, S., Millett, M., Paroli, L., Strutt, K., 2005. Portus: an archaeological survey of the port
979 of imperial Rome. British School at Rome.
980 Le Gall, J., 1953. Le Tibre, fleuve de Rome dans l'Antiquité. Presses universitaires de France,
981 Paris.
982 Le Roux, G., Véron, A., Morhange, C., 2005. Lead pollution in the ancient harbours of
983 Marseilles. Méditerranée 31–35.
984 Le Roux, G., Veron, A., Morhange, C., 2003. Geochemical evidences of early anthropogenic
985 activity in harbour sediments from Sidon. Archaeology & history in Lebanon 18, 115–
986 119.
987 Livy, T., 1997. History of Rome, Loeb Classical Library. Cambridge.
988 Mariotti Lippi, M., Bellini, C., Trinci, C., Benvenuti, M., Pallecchi, P., Sagri, M., 2007.
989 Pollen analysis of the ship site of Pisa San Rossore, Tuscany, Italy: the implications
990 for catastrophic hydrological events and climatic change during the late Holocene.
991 Veget Hist Archaeobot 16, 453–465.
992 Marriner, N., Morhange, C., 2006. Geoarchaeological evidence for dredging in Tyre's ancient
993 harbor, Levant. Quaternary Research 65, 164–171.
994 Marriner, N., Morhange, C., 2007. Geoscience of ancient Mediterranean harbours. Earth-
995 Science Reviews 80, 137–194.
996 Martin, J.-M., Whitfield, M., 1983. The Significance of the River Input of Chemical Elements
997 to the Ocean, in: Trace Metals in Sea Water, NATO Conference Series. Springer,
998 Boston, MA, pp. 265–296.
999 Martin, R., 1996. Un saggio sulle mura del castrum di Ostia (Reg. I, ins. X.3), in: "Roman
1000 Ostia" Revisited. Archaeological and Historical Papers in Memory of Russell Meiggs.
1001 Zevi, A.G., Claridge, A., Rome, pp. 19–38.
1002 Mattei, M., Conticelli, S., Giordano, G., 2010. The Tyrrhenian margin geological setting:
1003 from the Apennine orogeny to the K-rich volcanism, in: The Colli Albani Volcano,
1004 Special Publications of the International Association of Volcanology and Chemistry of
1005 the Earth's Interior. The Geological Society, London, pp. 7–27.
1006 Mazzini, I., Faranda, C., Giardini, M., Giraudi, C., Sadori, L., 2011. Late Holocene
1007 palaeoenvironmental evolution of the Roman harbour of Portus, Italy. Journal of
1008 Paleolimnology 46, 243–256.
1009 Milli, S., D'Ambrogi, C., Bellotti, P., Calderoni, G., Carboni, M.G., Celant, A., Di Bella, L.,
1010 Di Rita, F., Frezza, V., Magri, D., Pichezzi, R.M., Ricci, V., 2013. The transition from
1011 wave-dominated estuary to wave-dominated delta: The Late Quaternary stratigraphic
1012 architecture of Tiber River deltaic succession (Italy). Sedimentary Geology 284, 159–
1013 180.
1014 Minoura, K., Imamura, F., Takahashi, T., Shuto, N., 1997. Sequence of sedimentation
1015 processes caused by the 1992 Flores tsunami: Evidence from Babi Island. Geology 25,
1016 523–526.

Morhange, C., 1994. La mobilité des littoraux provençaux: Eléments d'analyse géomorphologique. Université de Provence, Aix-en-Provence.
Morhange, C., Blanc, F., Bourcier, M., Carbonel, P., Prone, A., Schmitt- Mercury, S., Vivent, D., Hesnard, A., 2003. Bio-sedimentology of the late Holocene deposits of the ancient harbor of Marseilles (southern France Mediterranean sea). The Holocene 13, 593–604.
Morhange, C., Laborel, J., Hesnard, A., 2001. Changes of relative sea level during the past 5000 years in the ancient harbor of Marseilles, Southern France. Palaeogeography, Palaeoclimatology, Palaeoecology 166, 319–329.
Morton, R.A., Gelfenbaum, G., Jaffe, B.E., 2007. Physical criteria for distinguishing sandy tsunami and storm deposits using modern examples. Sedimentary Geology, Sedimentary Features of Tsunami Deposits - Their Origin, Recognition and Discrimination: An Introduction 200, 184–207.
Reinhardt, E.G., Patterson, R.T., Blenkinsop, J., Raban, A., 1998. Paleoenvironmental evolution of the inner basin of the ancient harbor at Caesarea Maritima, Israel; foraminiferal and Sr isotopic evidence. Revue de Paleobiologie 17, 1–21.
Reinhardt, E.G., Patterson, R.T., Schröeder-Adams, C.J., 1994. Geoarchaeology of the ancient harbor site of Caesarea Maritima, Israel; evidence from sedimentology and paleoecology of benthic foraminifera. Journal of Foraminiferal Research 24, 37–48.
Reinhardt, E.G., Raban, A., 1999. Destruction of Herod the Great's harbor Caesarea Maritima, Israel, geoarchaeological evidence. Geology 27, 811–814.
Rescanières, S., 2002. Essai sur le cadre géographique antique du Narbonnais, in: Narbonne et Le Narbonnais, Carte Archéologique de La Gaule. Dellong, E., Paris, pp. 44–51.
Rita, F.D., Celant, A., Magri, D., 2010. Holocene environmental instability in the wetland north of the Tiber delta (Rome, Italy): sea-lake-man interactions. J Paleolimnol 44, 51–67.
Rossi, V., Sammartino, I., Amorosi, A., Sarti, G., De Luca, S., Lena, A., Morhange, C., 2015. New insights into the palaeoenvironmental evolution of Magdala ancient harbour (Sea of Galilee, Israel) from ostracod assemblages, geochemistry and sedimentology. Journal of Archaeological Science 54, 356–373.
Sadori, L., Mazzini, I., Pepe, C., Goiran, J.-P., Pleuger, E., Ruscito, V., Salomon, F., Vittori, C., 2016. Palynology and ostracodology at the Roman port of ancient Ostia (Rome, Italy). The Holocene 26, 1502–1512.
Sageman, B.B., Lyons, T.W., 2003. Geochemistry of fine-grained sediments and sedimentary rocks. Treatise on geochemistry 7, 115–158.
Salomon, F., 2013. Géoarchéologie du delta du Tibre. Lumière Lyon 2.
Salomon, F., Goiran, J.-P., Noirot, B., Pleuger, E., Bukowiecki, E., Mazzini, I., Carbonel, P., Gadhoum, A., Arnaud, P., Keay, S., Zampini, S., Kay, S., Raddi, M., Ghelli, A., Pellegrino, A., Morelli, C., Germoni, P., 2018. Geoarchaeology of the Roman port-city of Ostia: Fluvio-coastal mobility, urban development and resilience. Earth-Science Reviews 177, 265–283.
Salomon, F., Goiran, J.-P., Pannuzi, S., Djerbi, H., Rosa, C., 2017. Long-Term Interactions between the Roman City of Ostia and Its Paleomeander, Tiber Delta, Italy. Geoarchaeology 32, 215–229. https://doi.org/10.1002/gea.21589
Salomon, F., Keay, S., Carayon, N., Goiran, J.-P., 2016. The Development and Characteristics of Ancient Harbours—Applying the PADM Chart to the Case Studies of Ostia and Portus. PLoS One 11.
Salomon, P., Delile, H., Goiran, J.-P., Bravard, J.-P., Keay, S., 2012. The Canale di Comunicazione Traverso in Portus: the Roman sea harbour under river influence (Tiber delta, Italy). Géomorphologie: relief, processus, environnement, 75–90.
Sánchez Vizcaíno, A., Cañabate, M.L., 1999. Identification of activity areas by soil

phosphorus and organic matter analysis in two rooms of the Iberian Sanctuary "Cerro El Pajarillo." Geoarchaeology 14, 47–62.
Shumilovskikh, L.S., Seeliger, M., Feuser, S., Novenko, E., Schlütz, F., Pint, A., Pirson, F., Brückner, H., 2016. The harbour of Elaia: A palynological archive for human environmental interactions during the last 7500 years. Quaternary Science Reviews 149, 167–187.
Stanley, J.-D., Carlson, R.W., Van Beek, G., Jorstad, T.F., Landau, E.A., 2007. Alexandria, Egypt, before Alexander the Great: A multidisciplinary approach yields rich discoveries. GSA Today 17, 4–10.
Stock, F., Kerschner, M., Kraft, J.C., Pint, A., Frenzel, P., Brückner, H., 2014. The palaeo-geographies of Ephesos (Turkey), its harbours and the Artemision - a geoarchaeological reconstruction for the timespan 1500 - 300 BC. Zeitschrift für Geomorphologie 58, 33–66.
Stock, F., Knipping, M., Pint, A., Ladstätter, S., Delile, H., Heiss, A.G., Laermanns, H., Mitchell, P.D., Ployer, R., Steskal, M., Thanheiser, U., Urz, R., Wennrich, V., Brückner, H., 2016. Human impact on Holocene sediment dynamics in the Eastern Mediterranean – the example of the Roman harbour of Ephesus. Earth Surf. Process. Landforms 41, 980–996.
Stock, F., Pint, A., Horejs, B., Ladstätter, S., Brückner, H., 2013. In search of the harbours: New evidence of Late Roman and Byzantine harbours of Ephesus. Quaternary International 312, 57–69.
Strabo, 1924. Geography, Loeb Classical Library. Cambridge, translated by H. L. Jones.
Stumpf, R., Frank, M., Schönfeld, J., Haley, B.A., 2010. Late Quaternary variability of Mediterranean Outflow Water from radiogenic Nd and Pb isotopes. Quaternary Science Reviews 29, 2462–2472.
Thomas, M.F., Thorp, M.B., 1993. The geomophology of some Quaternary placers deposits. Zeitschrift für Geomorphologie 183‑194.
Tomassetti, G., 1897. Della Campagna romana nel medioveo. Archiv. della Soc. Romana Storia Patria (ASRSP) 20, 45–94.
Ventriglia, U., 1971. La geologia della citta di roma.
Véron, A., Goiran, J.P., Morhange, C., Marriner, N., Empereur, J.Y., 2006. Pollutant lead reveals the pre-Hellenistic occupation and ancient growth of Alexandria, Egypt. Geophysical Research Letters 33, 1–4.
Véron, A., Morhange, C., Poirier, A., Angeletti, B., Bertoncello, F., 2018. Geochemical markers of human occupation in the lower Argens valley (Fréjus, France): from protohistory to Roman times. Journal of Archaeological Science: Reports 17, 242–249.
Véron, A.J., Flaux, C., Marriner, N., Poirier, A., Rigaud, S., Morhange, C., Empereur, J.-Y., 2013. A 6000-year geochemical record of human activities from Alexandria (Egypt). Quaternary Science Reviews 81, 138–147.
Vittori, C., Mazzini, I., Salomon, F., Goiran, J.-P., Pannuzi, S., Rosa, C., Pellegrino, A., 2015. Palaeoenvironmental evolution of the ancient lagoon of Ostia Antica (Tiber delta, Italy). Journal of Archaeological Science 54, 374–384.
Vött, A., 2007. Silting up Oiniadai's harbours (Acheloos River delta, NW Greece). Geoarchaeological implications of late Holocene landscape changes. Géomorphologie : relief, processus, environnement 13.
Vött, A., Bareth, G., Brückner, H., Lang, F., Sakellariou, D., Hadler, H., Ntageretzis, K., Willershäuser, T., 2011. Olympia's Harbour Site Pheia (Elis, Western Peloponnese, Greece) Destroyed by Tsunami Impact. DIE ERDE – Journal of the Geographical Society of Berlin 142, 259–288.

Wunderlich, T., Wilken, D., Erkul, E., Rabbel, W., Vött, A., Fischer, P., Hadler, H., Heinzelmann, M., 2018. The river harbour of Ostia Antica - stratigraphy, extent and harbour infrastructure from combined geophysical measurements and drillings. Quaternary International 473, 55-65.
Zevi, F., 2002. Origini di Ostia, in: Ostia e Portus Nelle Loro Relazioni Con Roma, Istitutum Romanum Finlandiae. Bruun, C., Zevi, A.G., Rome, pp. 11–32.
Zevi, F., 2001. Ostie sous la République., in: Ostia, Port et Porte de La Rome Antique. Descoeudres, J.P., Genève, pp. 10–18.

Figure captions

Figure 1. (**A**) Location of the harbor basins of *Portus* and Ostia in the Tiber delta and position of cores PO2 and PTXI-3 (orange circles) analyzed in this work, and core TR14 analyzed by Delile et al. (2014a) (beige circle). (**B**) Map showing the archeological area of ancient Ostia with the location of core PO2, as well as the old (before AD 1557) and current Tiber river courses (modified from Gorian et al., 2014). The blue area is the location of the Ostia Antica harbor basin.

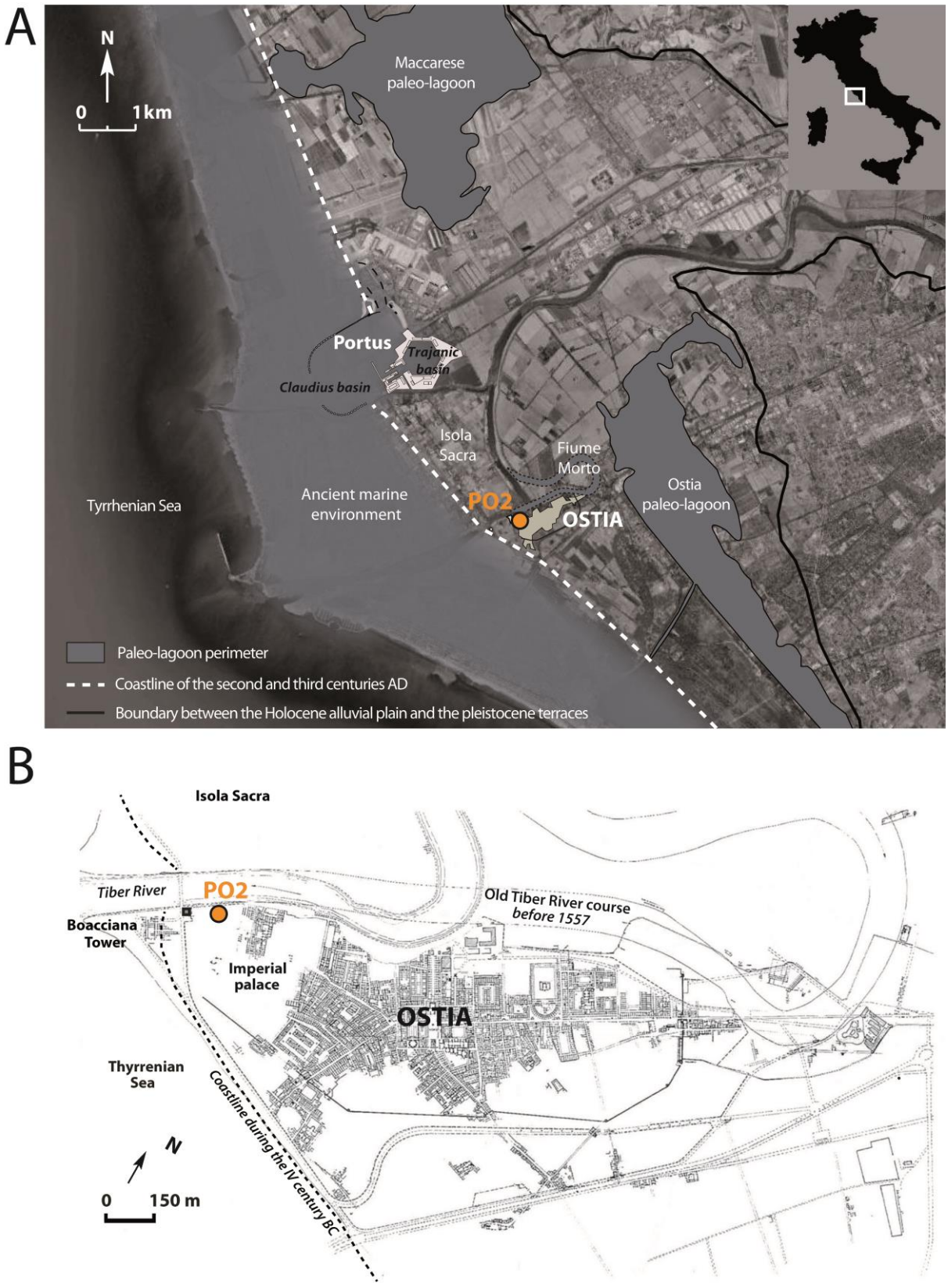

Figure 2. Stratigraphic log of core PO2 showing the age-depth model, stratigraphic and environmental descriptions, magnetic susceptibility values, the 50 percentile (D 50) grain

size, the granulometric diagram, Loss on Ignition (L.O.I.), $CaCO_3$ content, and ostracod assemblages divided into five ecological groups: marine, phytal marine, coastal phytal (i.e. phytal species requiring algae or higher plants for their life cycle), brackish lagoonal, and freshwater (modified from Gorian et al., 2014).

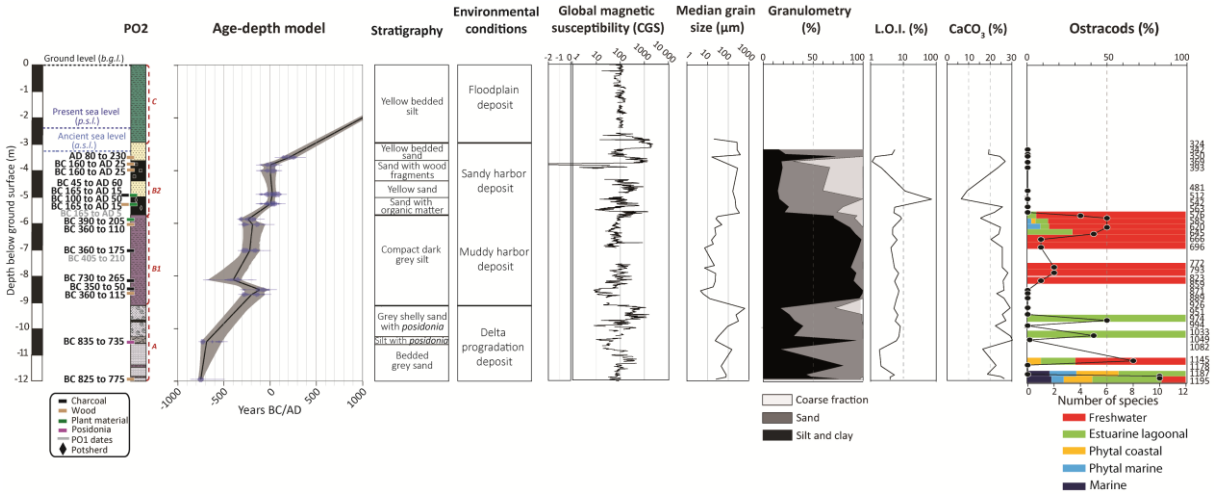

Figure 3. Geochemical logs of elemental concentrations of the PO2 core classified according to their supposed belonging to the main geochemical fluxes: (A) Detrital elements, (B) Authigenic elements, (C) Biogenic elements. Section 4.1.1. discusses how this approach of classifying elements according to their presumed affiliation with the main geochemical inputs is arbitrary.

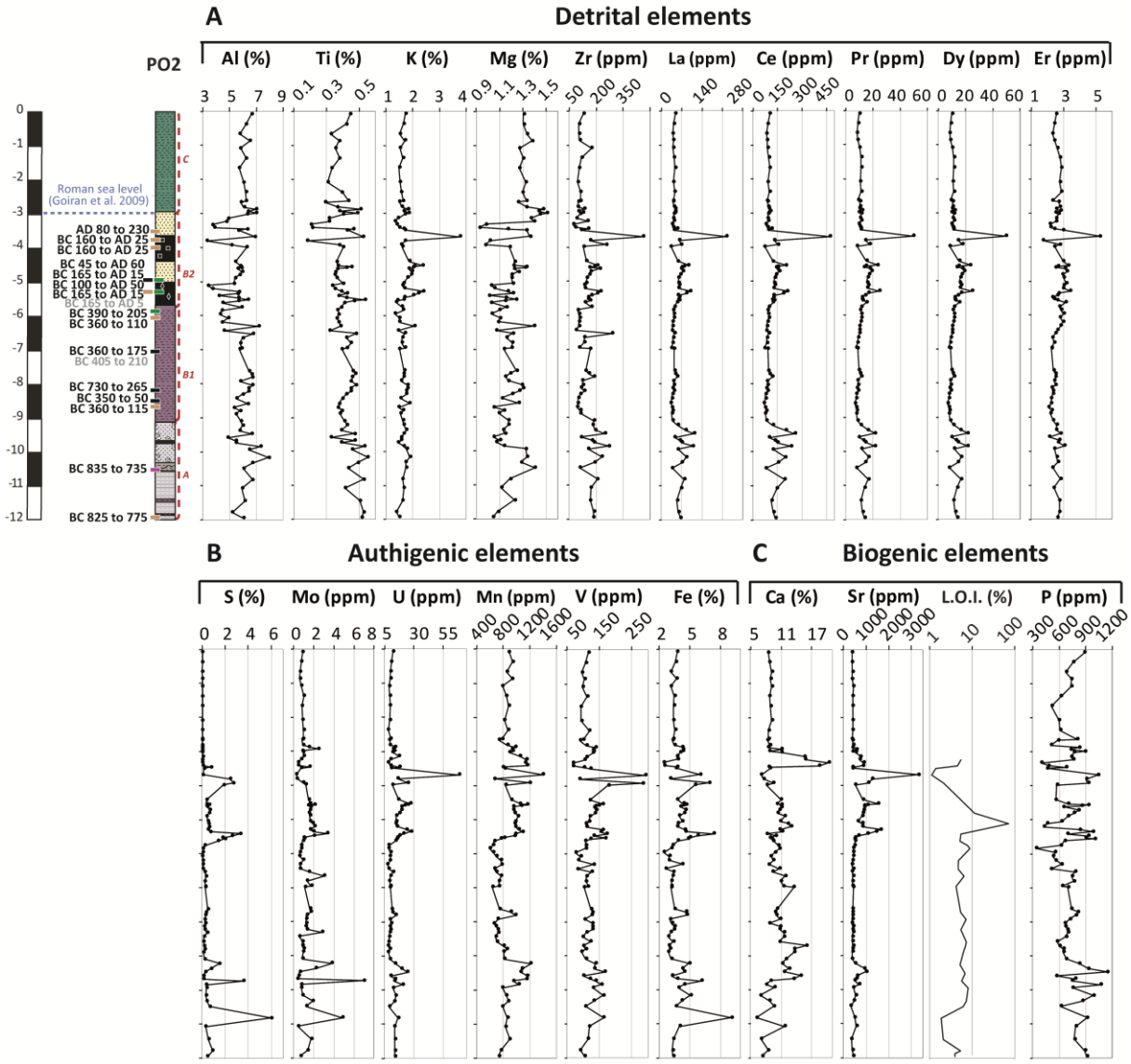

1147

1148 **Figure 4**. (**A**) Factor analysis of elemental concentrations in core PO2. The number of factors
1149 is limited to four: (1) Silicate detrital fraction (47%); (2) aluminosilicate detrital fraction
1150 versus carbonate fraction (13%); (3) anoxic conditions (10%); (4) seawater influence versus
1151 polluted freshwater (7%). (**B**) Distribution of the different factors with depth in the column.
1152 The gray and white shadings and the gray dotted line highlight the main geochemical units of
1153 the core discussed in section 4.4.

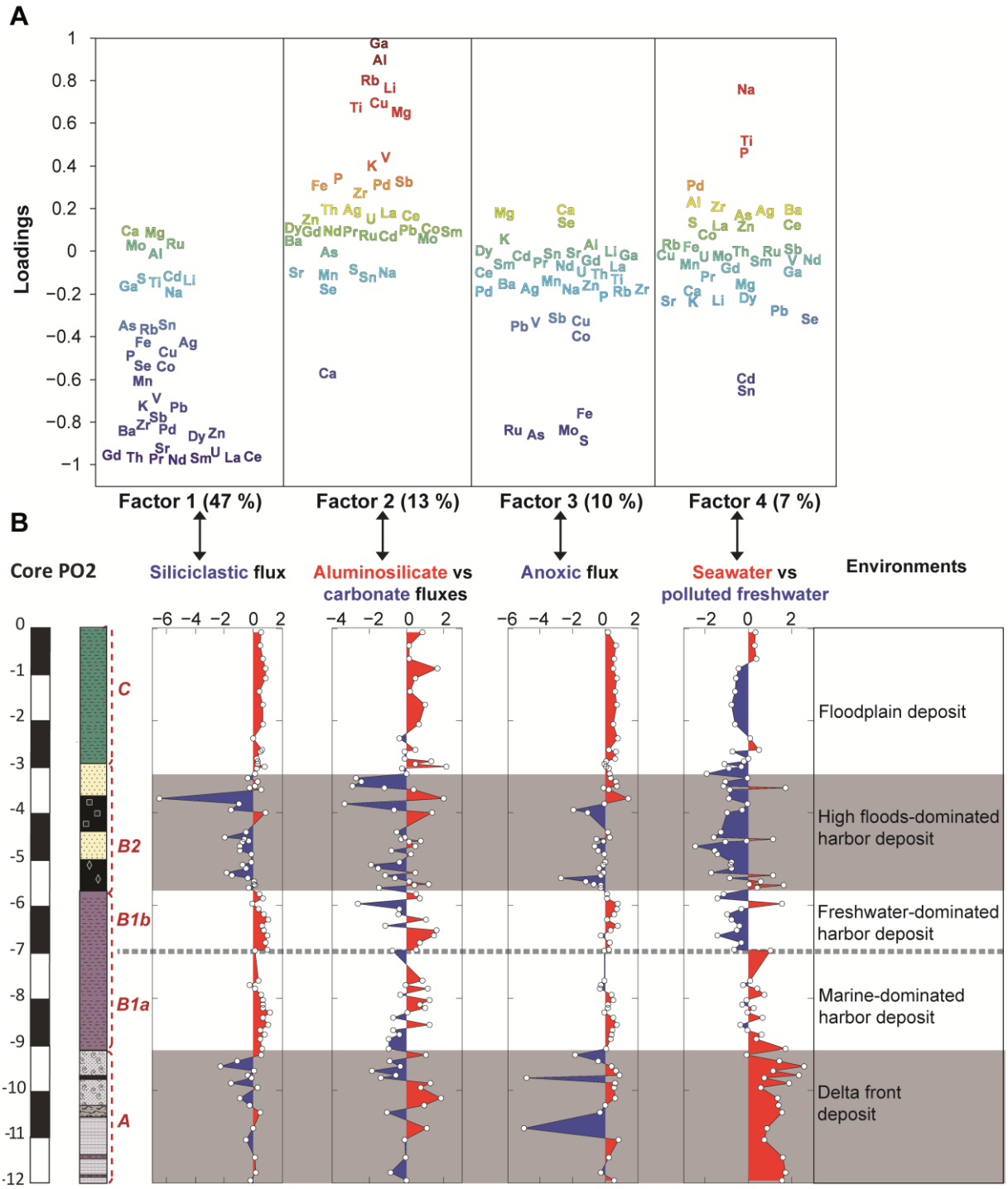

Figure 5. (A) Lead isotope ratios ($^{204}Pb/^{206}Pb$ vs. $^{208}Pb/^{206}Pb$) and (B) geochemical parameters (T_{mod} vs. κ) for leachates from the uncontaminated sediments of the *Trajanic* (in red), Claudian (in yellow), and Ostia (in green) harbor deposits, and of the *Canale Romano* (in blue). Together, these samples define a geological mixing line between the α' component composed of volcanic rocks from the Alban Hills (Conticelli et al., 2002; D'Antonio et al.,

1996) and the α" component related to the erodible recent Apennine limestones, which are very similar to Pb dissolved in modern Mediterranean seawater (Stumpf et al., 2010) (modified from Delile et al., 2017).

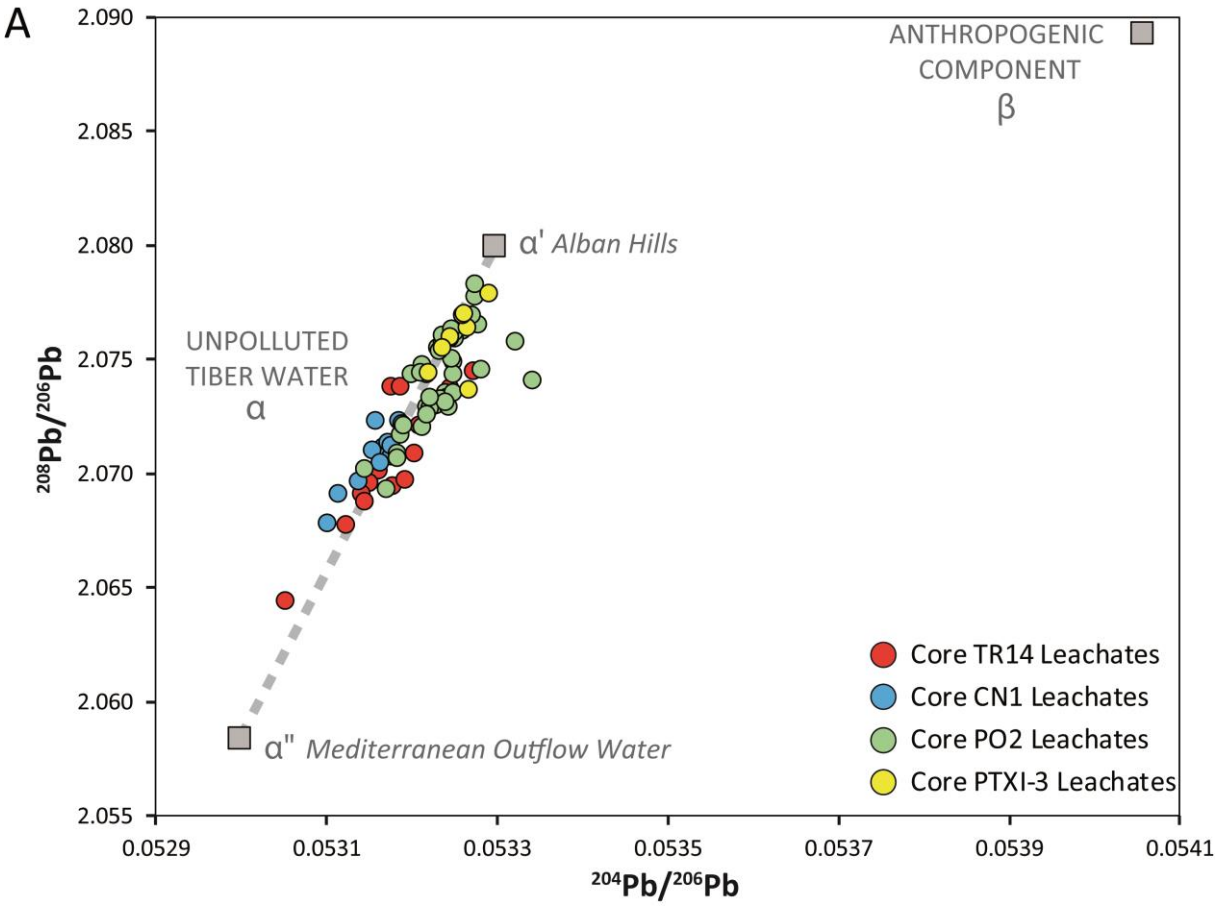
A
ANTHROPOGENIC COMPONENT
β
α' Alban Hills
UNPOLLUTED TIBER WATER
α
α" Mediterranean Outflow Water
Core TR14 Leachates
Core CN1 Leachates
Core PO2 Leachates
Core PTXI-3 Leachates
208Pb/206Pb
204Pb/206Pb
2.090
2.085
2.080
2.075
2.070
2.065
2.060
2.055
0.0529
0.0531
0.0533
0.0535
0.0537
0.0539
0.0541

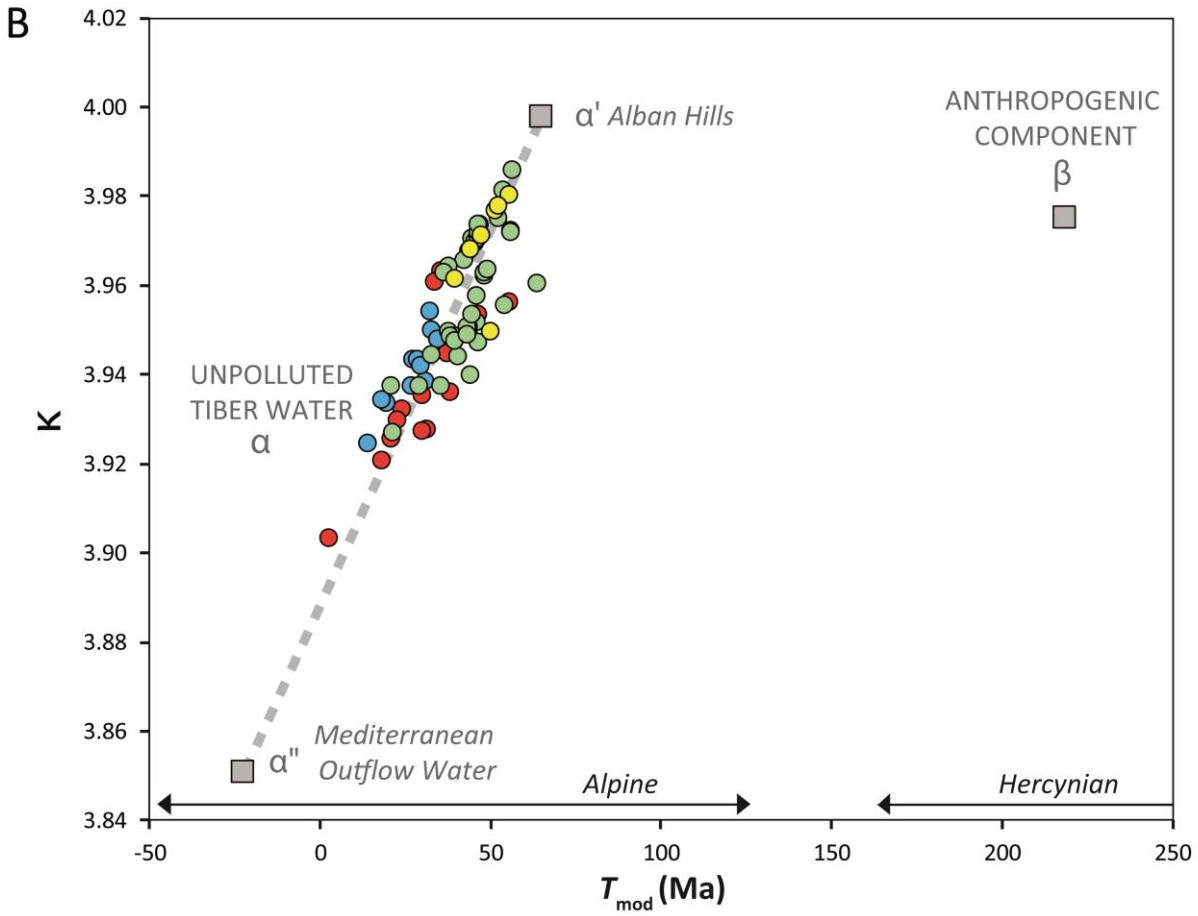
B
ANTHROPOGENIC COMPONENT
β
α' Alban Hills
UNPOLLUTED TIBER WATER
α
α" Mediterranean Outflow Water
Alpine
Hercynian
K
Tmod (Ma)
4.02
4.00
3.98
3.96
3.94
3.92
3.90
3.88
3.86
3.84
-50
0
50
100
150
200
250

1163

Figure 6. Plot of *f*α' and *f*α" values (proportion of the natural sub-components α' and α" in all uncontaminated sediment samples) against sand, silt, and clay percentages for leachates (in green) and residues (in black) from core TR 14 and leachates from cores PTXI-3 (in grey) and PO2 (in yellow).

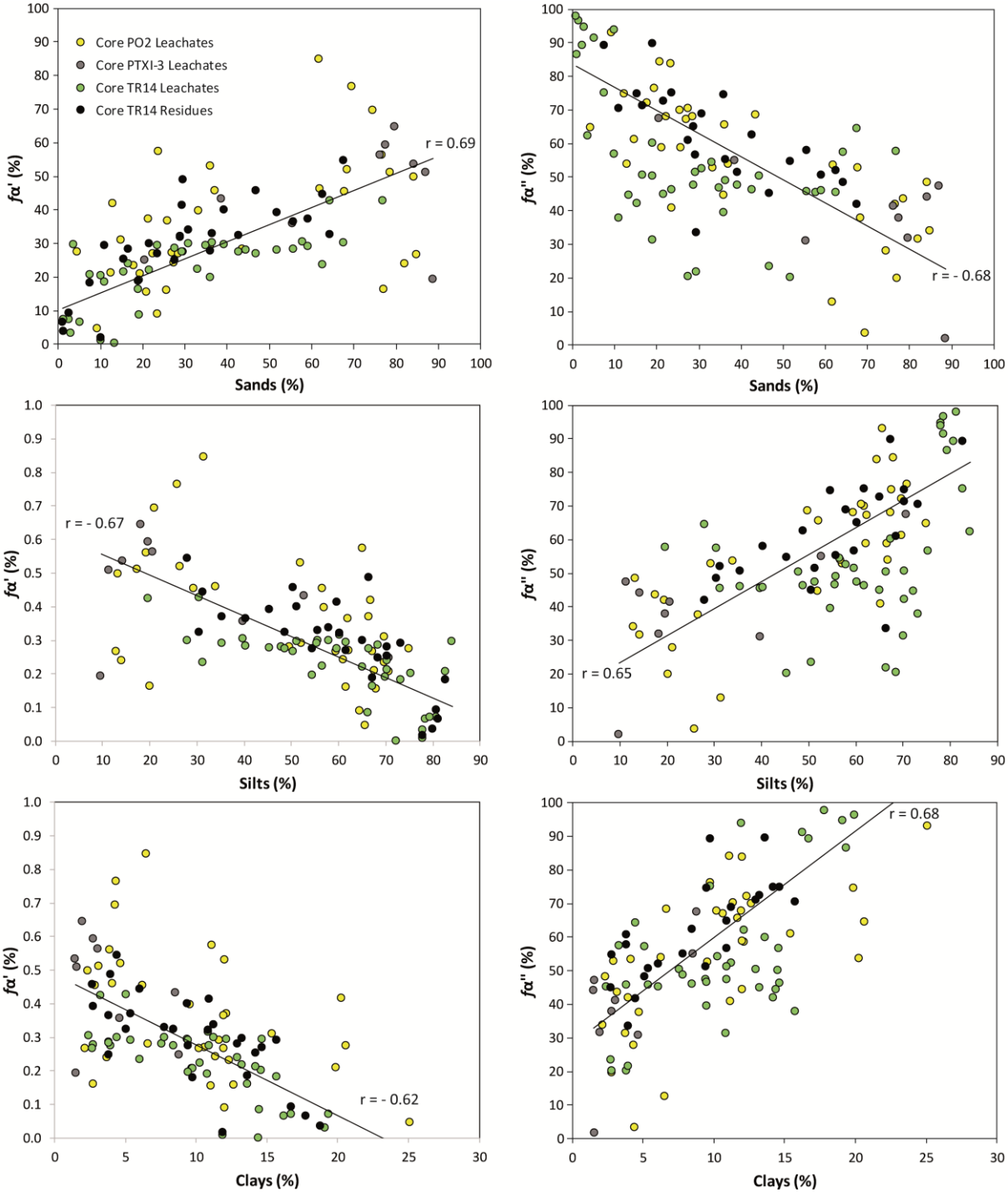

Table 1. Environmental factors involved in the formation of sedimentary deposits in the ancient harbor basins of Ostia (Factor analysis in Fig. 4), Claudius (Factor analysis in Fig. S4 and data in Table S1), Trajan, Ephesus, and Naples. These environmental variables, organized in order of relative importance, have been identified by factor analysis of element concentrations. For each of these variables, the chemical elements concerned, the associated processes, and the types of environments involved are given.

			ENVIRONMENTAL FACTORS SORTED ACCORDING TO THEIR SIGNIFICANCE (F1 TO F4 IN %) AND INFERRED FROM FACTOR ANALYSIS						
Harbor site	**Reference**	**Coastal geomorphology**	**Detrital flux (42%)**	**Biogenic flux (34%)**	**Oxic condition (20%)**	**Anoxic condition (20%)**	**Mineralogy/lithology (11%)**	**Anthropogenic flux (10%)**	**Seawater flux (8%)**
Ostia	This study	Delta	F1 (47 %)	N/A	F3 (10 %)	F3 (10 %)	F2 (13 %)	F4 (10 %)	F4 (7 %)
Portus (Trajanic basin)	Delile et al. (2014a)	Delta	F1 (55 %)	F1 (55 %)	F2 (17 %)	F2 (17 %)	N/A	F4 (5 %)	F3 (9 %)
Portus (Claudius basin)	This study	Delta	F1 (44 %)	F2 (16 %)	N/A	N/A	F3 (12 %)	N/A	F4 (6 %)
Ephesus	Delile et al. (2015)	Delta	F1 (49 %)	F1 (49 %)	F2 (19 %)	F2 (19 %)	F3 (8 %)	N/A	N/A
Naples	Delile et al. (2016a)	Coastal bay	F2 (16 %)	F2 (16 %)	F1 (36 %)	F1 (36 %)	F3 (10 %)	F2 (16 %)	F3 (10 %)
SYNTHESIS		**Significant elements**	Al, Zr, Ti, Th, Mg, Ba, K, Co, Zn, REEs	LOI, Ca, Sr	Mn, K, Ti, Zn Cr, Co, Cd	S, Mo, U, Pb, Ag, Cu	Al, Rb, La, Se, Ce, Ga, Li, Be, Zr, K, Ti, Mg	Pb, Ag, Sn, Cu, Cd,	Na
		Process	Fluvial hydrodynamics: - Canal networks - Coastal and delta progradation	Biomass production: - Organic matter - Skeletal remains - Eutrophication - Urban sewage inputs	- Delta progradation - Swell	-Enclosing harbor basin -Weak water-column ventillation -Interflood period -Urban sewage inputs and eutrophication	- Erosion of the local and regional geological basement	- Heavy metal inputs - Using of lead pipe networks - Metallurgic activities	- Seawater influence - Infiltration of the littoral salt wedge
		Paleo-environment	- Floodplain - Freshwater-dominated harbor - Coastal alluvial fan - Paleo-channel - Delta front - Prodelta environment	- Swamp - Marine - Enclosed harbor - Peat - Lagoonal - Brackish and eutrophic environments	- Floodplain - Freshwater-dominated harbor - Coastal alluvial fan - Paleo-channel - Delta front - Prodelta environments - Beach	- Marine - Enclosed harbor - Peat - Lagoonal - Swamp	In all environments	In all environments	- Marine dominated harbor - Delta front

1175

Figure S1. Color-coded correlation matrix (correlogram) for all measured chemical elements in core PO2.

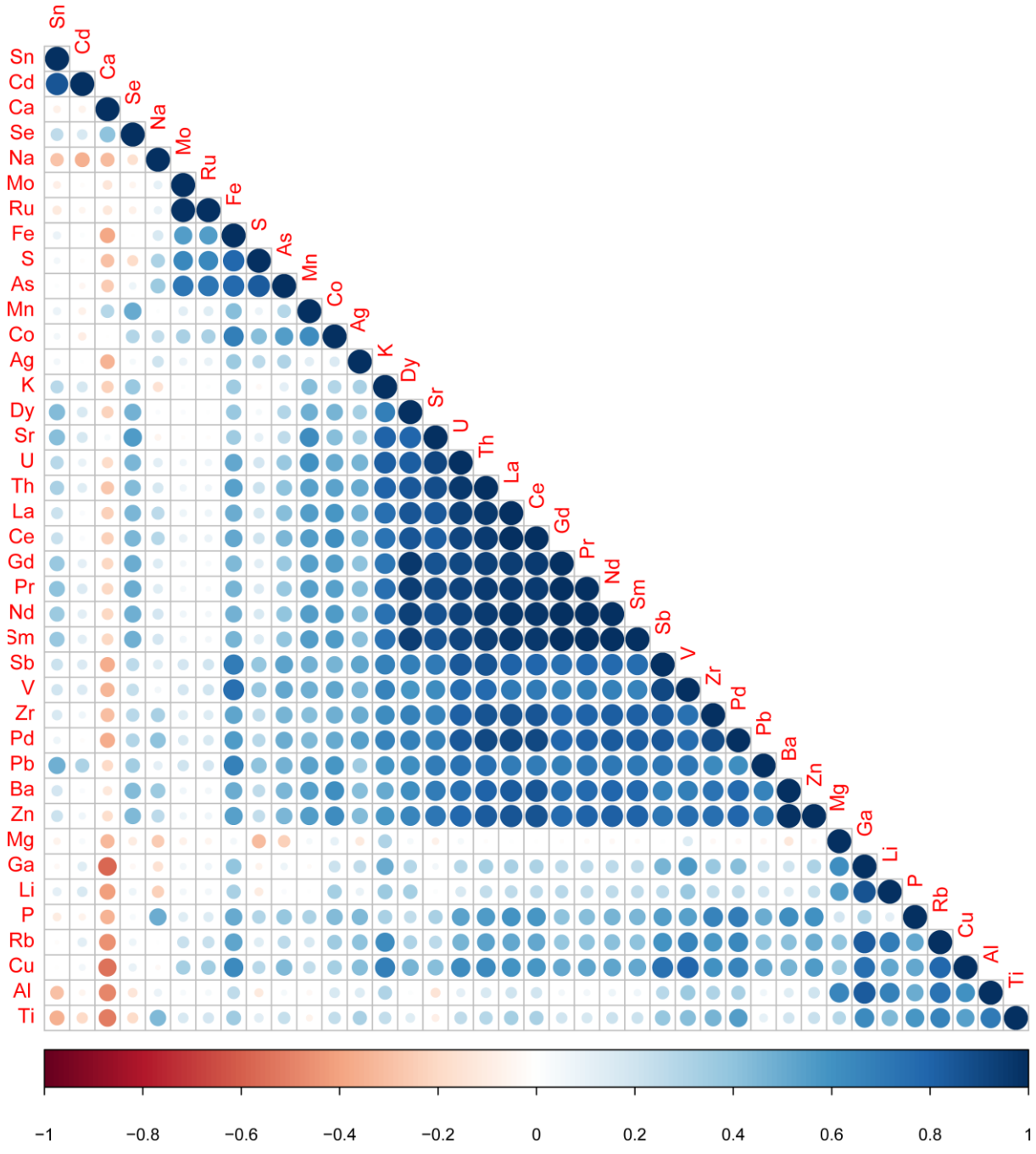

Figure S2. Color-coded correlation matrix (correlogram) for all measured chemical elements and granulometric fractions in the harbor subunits B1 and B2 of core PO2. Two groups have been identified by hierarchical clustering.

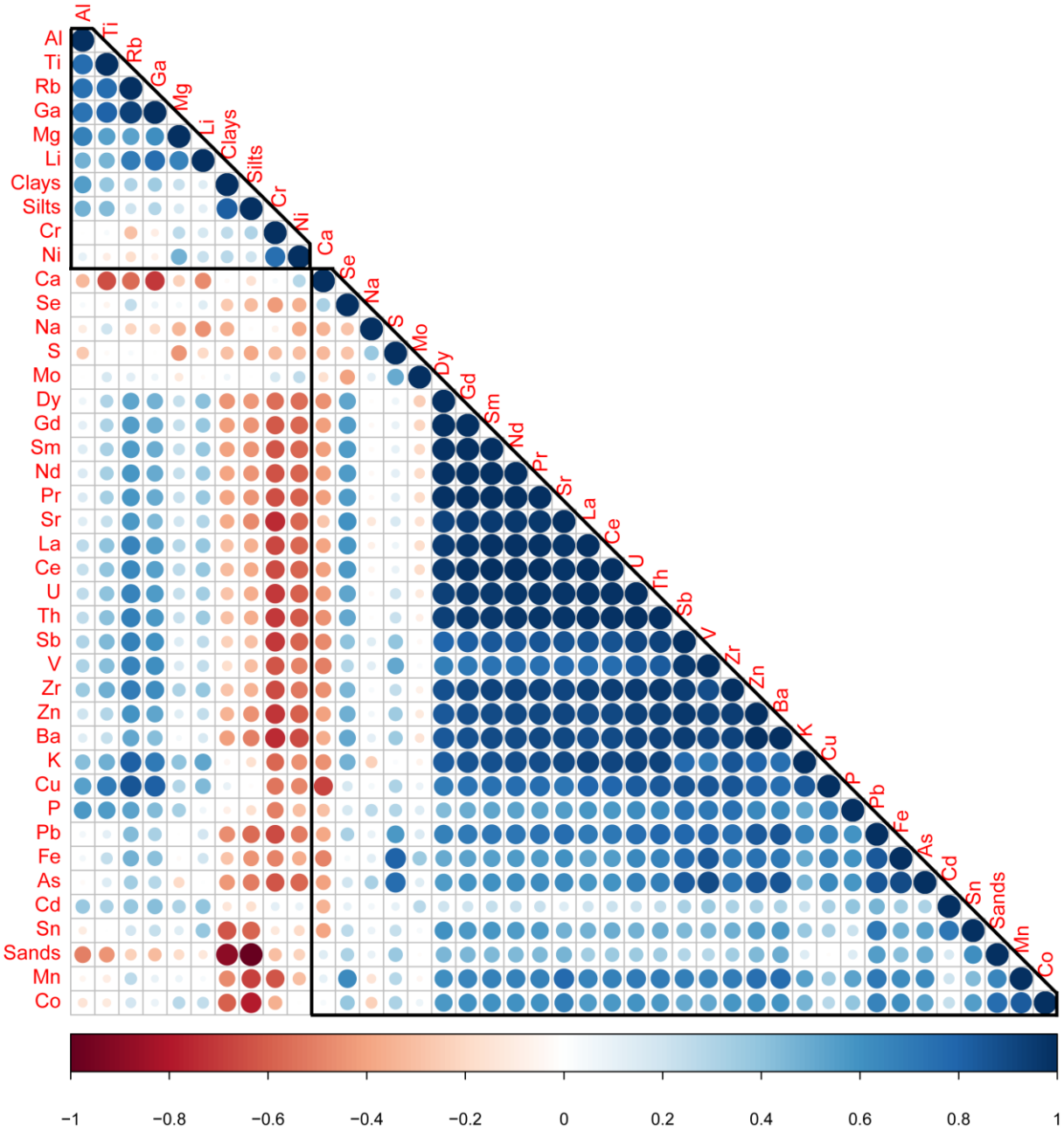

1183

1184 **Figure S3**. (**A**) Photo showing subhorizontal bedding formed by placers on the current

1185 coastline of the Tiber delta (modified from Salomon, 2013). (**B**) Close-up of a

1186 pluricentimetric layer containing placers.

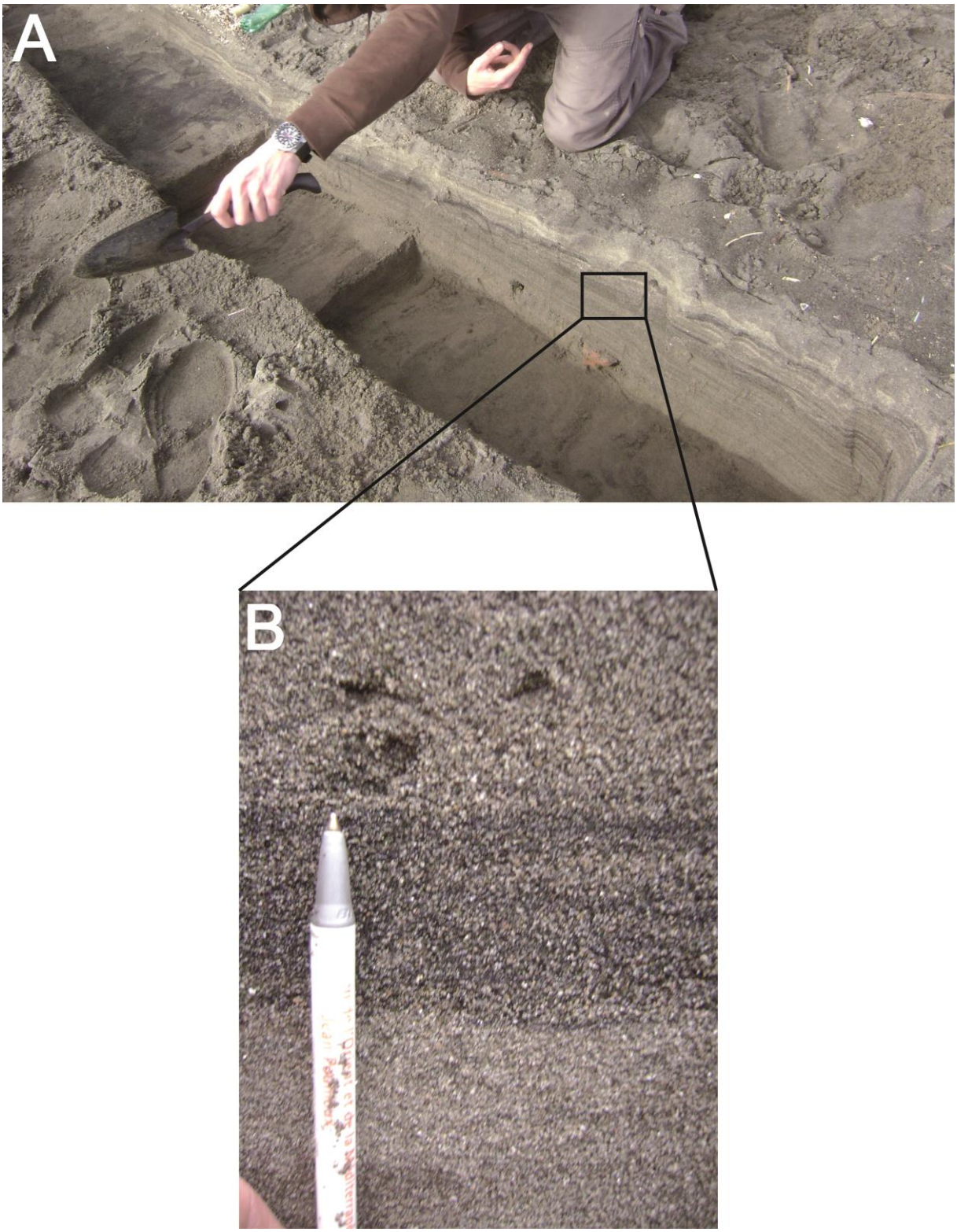

Figure S4. (**A**) Factor analysis of elemental concentrations in core PTXI-3 taken in the ancient harbor basin of Claudius. The number of factors is limited to four: (1) Silicate detrital

fraction (44%); (2) biogenic fraction (16%); (3) aluminosilicate detrital fraction (12%); (4) seawater influence (6%). (**B**) Distribution of the different factors with depth in the column.

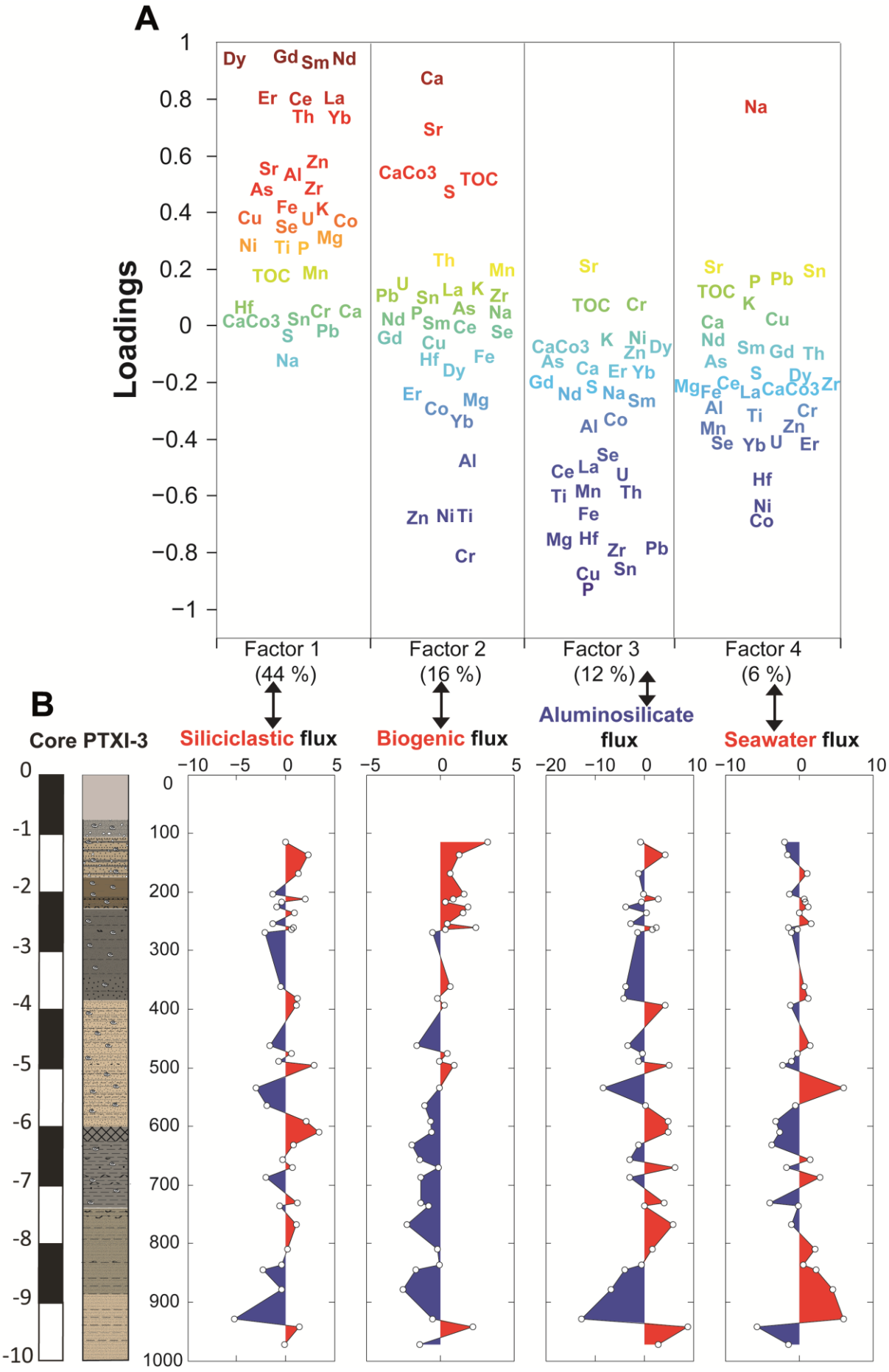
A
Loadings
Factor 1 (44 %)
Factor 2 (16 %)
Factor 3 (12 %)
Factor 4 (6 %)
B
Core PTXI-3
Siliciclastic flux
Biogenic flux
Aluminosilicate flux
Seawater flux

Table S1. Major and trace element concentrations in core PTXI-3. Values in wt.% for major elements and in ppm for trace elements.

			wt.%										ppm																				
Depth (cm)	L.O.I.	CaCo3	Al_2O_3	Fe_2O_3	CaO	Na_2O	K_2O	MgO	TiO_2	P_2O_5	MnO	SO_2	Zr	Cr	Co	Ni	Cu	Zn	As	Se	Sr	Sn	La	Ce	Nd	Sm	Gd	Dy	Er	Yb	Hf	Pb	Th	U
115	5	33	8.76	3.37	19.66	1.28	2.15	1.49	0.30	0.14	0.10	0.39	146.16	34.88	13.64	28.65	25.72	41.07	28.02	9.86	652.26	2.94	57.31	111.69	49.62	8.62	6.91	4.48	2.30	1.92	161.11	44.12	25.89	3.16
136	6	40	7.84	2.63	20.67	1.42	2.09	1.37	0.24	0.10	0.12	0.41	121.39	35.68	12.24	31.88	25.10	52.89	22.17	3.22	981.79	2.73	52.05	100.85	54.40	9.88	7.41	5.23	2.43	1.88	59.21	47.06	23.72	3.29
169	30	13	8.25	2.36	17.88	1.46	2.20	1.26	0.27	0.11	0.12	0.78	134.73	38.27	7.11	23.51	29.19	57.61	17.48	4.69	1037.52	3.81	56.46	112.99	61.41	10.94	8.65	6.00	2.76	2.42	63.92	55.27	26.82	4.38
205	8	26	6.26	3.93	18.14	1.01	1.51	0.91	0.22	0.09	0.10	11.14	139.48	29.97	9.63	22.03	20.40	35.09	19.90	7.80	577.20	1.07	36.17	70.02	32.11	5.92	4.83	3.45	1.81	1.59	127.19	38.09	16.41	2.68
213	14	23	9.08	3.80	16.51	1.53	2.45	1.03	0.23	0.10	0.07	0.84	84.42	37.02	9.39	26.95	16.23	54.87	23.13	5.29	908.35	3.08	48.67	95.10	51.77	8.68	6.98	4.85	2.10	1.82	46.36	35.02	22.59	3.51
218	16	26	8.28	4.20	18.97	1.35	2.28	0.99	0.22	0.10	0.07	3.10	97.62	26.88	7.82	19.98	18.68	46.45	25.03	3.47	902.39	2.64	45.63	87.70	47.59	7.84	6.41	4.04	1.89	1.62	45.28	34.33	20.79	3.45
226	23	15	8.50	5.12	14.76	1.53	2.11	1.18	0.25	0.11	0.11	3.92	138.14	43.83	7.86	28.31	21.37	56.93	19.39	3.59	827.42	2.70	44.63	86.17	47.76	8.41	6.46	4.43	2.05	1.77	58.44	41.19	23.73	3.77
235	17	27	8.81	2.99	18.65	1.41	2.30	1.24	0.25	0.10	0.06	2.30	88.53	42.18	9.92	32.18	18.00	61.85	21.94	7.95	1073.60	3.31	51.25	98.90	55.19	9.53	7.46	4.87	2.34	1.85	53.49	38.47	23.36	3.74
255	2	34	8.40	2.65	17.00	1.49	2.37	1.06	0.23	0.10	0.06	1.74	88.06	27.78	8.53	19.94	15.64	44.85	20.43	3.90	842.42	4.40	41.52	81.16	42.96	7.73	6.35	4.04	1.82	1.55	44.53	39.55	18.95	6.41
262	11	28	9.15	3.46	17.78	1.40	2.32	1.31	0.30	0.11	0.14	2.08	111.33	34.77	13.28	25.11	13.54	40.69	19.01	6.56	609.94	1.18	45.82	87.19	40.23	7.02	5.42	3.84	1.83	1.52	137.32	36.62	21.38	8.71
265	4	33	8.74	3.40	15.39	1.45	2.24	1.25	0.27	0.10	0.06	2.65	97.61	43.23	9.17	25.41	19.58	56.97	18.58	5.96	758.57	3.59	43.56	83.38	48.71	8.19	6.38	4.40	2.11	1.80	53.04	37.13	19.52	4.98
270	13	26	8.35	2.92	17.10	1.45	2.29	1.18	0.26	0.11	0.12	1.89	98.31	28.42	10.42	19.22	11.40	34.98	12.76	6.90	567.53	1.48	37.20	73.88	32.21	5.86	4.71	3.40	1.61	1.25	110.13	36.47	18.09	5.51
362	7	25	9.19	5.77	19.91	1.58	1.63	2.14	0.48	0.27	0.14	3.98	204.82	41.62	12.54	24.44	73.43	54.09	16.69	8.05	571.24	111.75	60.79	124.43	53.74	9.44	6.97	4.33	2.00	1.71	215.25	2100.79	30.22	6.30
382	4	23	10.90	6.16	16.28	1.73	2.63	3.11	0.55	0.35	0.16	2.08	274.70	42.85	16.58	29.13	117.46	65.84	25.63	11.75	678.14	47.82	77.05	159.96	66.02	11.72	8.67	5.22	2.56	2.12	286.91	562.95	43.26	8.39
393	10	25	7.61	2.96	17.83	1.24	1.88	1.54	0.33	0.10	0.05	0.33	74.98	85.89	11.18	35.67	16.34	57.35	7.33	9.91	709.48	2.40	36.13	79.71	42.45	8.11	6.26	4.40	2.07	1.68	49.58	28.58	12.55	2.59
463	6	34	7.23	2.95	15.83	1.23	1.76	1.83	0.34	0.11	0.05	0.44	87.22	93.57	17.94	40.24	19.85	63.36	9.17	1.51	651.93	1.94	35.48	81.67	46.99	8.29	6.61	4.38	2.08	1.69	56.01	30.16	11.97	2.59
475	3	25	8.57	3.06	14.67	1.34	1.93	1.40	0.35	0.11	0.09	0.23	99.40	56.60	11.29	36.73	18.95	63.35	7.64	7.06	709.13	3.76	49.74	110.23	53.51	9.06	7.71	5.17	2.39	2.03	59.45	39.51	19.08	5.03
490	1	21	8.14	3.26	16.03	1.26	1.79	1.39	0.35	0.10	0.11	0.09	108.00	74.28	11.95	42.11	16.74	58.20	8.62	7.43	608.66	0.77	49.15	106.25	46.55	8.38	6.56	4.43	2.37	1.95	202.93	37.29	18.89	5.80
496	1	21	9.25	3.51	14.92	1.36	2.12	1.42	0.36	0.12	0.10	0.28	122.63	54.55	11.70	30.04	21.84	71.99	8.41	7.92	887.80	2.63	52.83	115.08	58.60	10.62	7.92	5.20	2.17	1.83	65.20	47.48	22.51	3.79
535	1	21	7.67	2.82	13.50	1.37	1.81	1.45	0.34	0.10	0.09	0.19	90.28	67.39	9.22	28.28	16.50	54.45	5.26	3.22	566.48	2.14	31.73	72.48	39.94	7.49	5.87	4.16	1.92	1.58	47.67	27.62	12.08	2.50
564	1	14	8.09	2.79	16.58	1.41	2.23	1.23	0.25	0.08	0.05	0.23	73.16	47.03	9.18	27.49	13.05	44.91	4.79	2.87	606.56	1.24	26.93	58.22	30.93	5.81	4.49	3.43	1.47	1.26	35.08	25.98	9.37	1.55
591	1	19	8.49	3.59	15.02	1.27	1.92	1.54	0.42	0.12	0.06	0.33	111.94	116.68	11.88	39.37	22.06	76.78	8.77	7.67	682.82	3.16	50.57	114.34	59.54	10.22	7.72	5.19	2.40	1.96	70.02	41.09	21.14	3.32
611	1	13	9.95	5.02	10.09	1.37	2.00	1.24	0.37	0.12	0.04	4.00	141.79	55.51	14.62	44.00	33.03	75.24	52.61	8.64	621.30	3.19	65.71	133.91	71.13	12.07	9.44	6.12	2.73	2.23	70.37	61.35	27.14	4.30
633	1	19	13.56	5.38	8.47	0.93	2.23	2.17	0.62	0.11	0.13	0.30	171.31	119.39	33.17	94.70	46.05	125.25	19.62	10.58	345.19	4.01	65.24	131.49	58.35	10.39	8.31	5.92	3.18	2.90	289.57	48.00	26.87	9.51
657	2	11	10.17	4.45	10.50	1.31	2.17	1.52	0.40	0.11	0.12	1.40	139.98	86.28	14.14	45.09	31.44	80.76	67.09	4.95	559.47	3.55	45.11	99.90	49.55	8.72	7.13	5.39	2.47	2.15	66.00	43.10	19.86	4.05
670	10	10	7.91	2.28	12.03	1.50	2.05	1.07	0.26	0.08	0.04	0.21	62.44	64.37	7.08	24.31	13.92	45.46	7.40	2.80	499.08	2.06	25.22	58.02	29.82	5.09	4.31	3.08	1.45	1.22	35.67	24.76	10.13	1.92
688	5	12	7.99	2.53	10.88	1.53	1.90	1.17	0.32	0.09	0.09	0.15	65.11	54.42	6.75	35.52	13.64	49.49	9.80	8.01	408.44	1.11	34.54	75.85	34.08	6.28	5.32	3.76	1.86	1.69	117.41	26.90	10.25	2.14
731	5	18	11.32	4.84	10.23	1.30	2.13	2.06	0.50	0.11	0.13	0.28	110.78	102.58	12.87	61.21	29.09	85.63	17.70	7.60	346.67	2.14	42.14	87.74	39.62	7.26	6.04	4.57	2.54	2.21	177.41	35.79	17.28	3.30
736	1	14	9.15	3.39	11.41	1.45	1.96	1.36	0.40	0.12	0.05	0.28	99.40	71.20	8.37	32.28	20.51	63.49	15.35	4.52	476.60	2.19	35.98	82.03	42.00	7.73	5.82	4.16	2.04	1.92	57.94	32.65	15.97	2.40
768	8	22	8.55	3.07	11.40	1.55	1.93	1.22	0.33	0.11	0.09	0.15	96.40	61.84	8.28	25.69	18.27	60.80	7.65	4.55	477.03	1.66	31.44	69.01	38.18	6.92	6.04	4.21	2.06	1.80	48.59	27.54	14.64	2.37
809	2	12	8.84	2.90	11.95	1.52	2.13	1.11	0.28	0.10	0.04	0.14	75.35	67.83	8.55	30.78	18.10	55.69	8.73	2.06	504.85	1.55	31.30	68.00	37.41	6.55	5.56	3.81	1.79	1.52	43.48	30.15	13.48	1.96
837	1	13	8.57	2.98	11.74	1.60	1.88	1.25	0.35	0.12	0.05	0.16	77.27	75.11	9.39	31.38	18.24	61.56	7.74	2.47	446.30	2.26	31.64	68.22	38.17	6.54	5.77	4.07	1.93	1.69	49.22	24.16	12.87	2.49
845	2	20	8.22	2.93	11.88	1.54	1.91	1.19	0.38	0.10	0.09	0.05	80.95	71.42	8.18	33.82	12.29	49.10	9.98	6.23	449.30	1.55	33.30	71.41	34.79	6.19	5.03	3.70	1.98	1.68	136.89	25.80	12.58	2.31
879	1	17	11.82	4.36	12.35	1.28	2.29	1.36	0.43	0.13	0.05	0.16	132.24	69.86	12.26	44.82	29.43	89.69	18.60	8.06	609.53	2.59	61.77	125.12	63.32	10.71	8.06	5.39	2.40	2.11	74.81	61.45	29.79	3.34
928	3	22	7.89	2.48	13.56	1.51	2.04	1.08	0.28	0.08	0.04	0.14	54.95	68.45	8.16	29.54	13.48	52.44	7.47	6.35	553.82	1.41	30.63	65.05	35.85	6.54	5.43	3.87	1.82	1.46	37.72	22.84	10.68	1.72
942	1	21	7.52	2.25	12.65	1.45	2.01	1.00	0.25	0.08	0.04	0.13	57.06	52.04	6.92	23.65	12.74	47.00	6.95	1.67	506.07	1.04	23.20	49.78	28.72	5.35	4.52	3.29	1.54	1.35	35.31	20.16	8.46	1.40
973	1	22	7.63	2.40	11.86	1.55	1.76	1.09	0.36	0.09	0.08	0.07	75.65	60.11	7.60	45.66	10.49	50.08	10.07	5.39	405.26	0.64	34.49	70.03	33.34	6.40	5.51	3.87	1.98	1.81	122.32	21.42	11.12	2.45

1195

1196

1197

1198